UHASSELT
KNOWLEDGE IN ACTION

Maastricht University

Faculty of Medicine and Life Sciences
School for Life Sciences
Master of Biomedical Sciences

Masterthesis

A closer look at chronic rejection in the murine model of orthotopic lung transplantation

Janne Kaes

Thesis presented in fulfillment of the requirements for the degree of Master of Biomedical Sciences, specialization Clinical Molecular Sciences

SUPERVISOR :
dr. Bieke BROUX

SUPERVISOR :
prof. dr. Bart VANAUDENAERDE

CO-SUPERVISOR :
dr. Stijn VERLEDEN

MENTOR :
drs. Tobias HEIGL

2017
2018

Transnational University Limburg is a unique collaboration of two universities in two countries: the University of Hasselt and Maastricht University.

UHASSELT
KNOWLEDGE IN ACTION

www.uhasselt.be
Universiteit Hasselt
Campus Hasselt:
Martelarenlaan 42 | 3500 Hasselt
Campus Diepenbeek:
Agoralaan Gebouw D | 3590 Diepenbeek

UHASSELT
KNOWLEDGE IN ACTION

Maastricht University

Faculty of Medicine and Life Sciences
School for Life Sciences
Master of Biomedical Sciences

Masterthesis

A closer look at chronic rejection in the murine model of orthotopic lung transplantation

Janne Kaes

Thesis presented in fulfillment of the requirements for the degree of Master of Biomedical Sciences, specialization Clinical Molecular Sciences

SUPERVISOR :
dr. Bieke BROUX

SUPERVISOR :
prof. dr. Bart VANAUDENAERDE

CO-SUPERVISOR :
dr. Stijn VERLEDEN

MENTOR :
drs. Tobias HEIGL

Preface

During the last eight months, I had the opportunity to complete my senior internship at the Lab of Pneumology at KU Leuven. I learned a lot about the fascinating world of lung transplantation and discovered many unanswered questions regarding this field. The past eight months were quite an experience with many educational and pleasant moments. Therefore, I would like to thank everyone who contributed and supported me during this period.

First of all, I would like to thank my promotor prof. dr. Bart Vanaudenaerde for the opportunities you gave me during the multiple summer jobs and especially during this internship. Thank you for stimulating me and providing the right feedback. I admire your scientific mind and ability to think outside the box.

Furthermore, I want to thank my co-promotor dr. Stijn Verleden for the useful input, valuable advice, guidance and correcting my thesis critically several times. Your passion and enthusiasm for research is a great example for many young scientists like me. I wish you all the best with your coming baby.

My daily supervisor, Tobias Heigl, thank you for all the effort you did to teach me the difficult microsurgical procedures. I respect your surgical skills and one day, I hope to be as good as you are. Thanks for your trust and believe in me during this learning process. I appreciate the useful input and corrections you had for this thesis.

I would like to thank the complete research group of lung transplantation for the ideas and suggestions during the several lab meetings.

Thanks to dr. Bieke Broux and prof. dr. Virginie Bito for reviewing my project and suggestions during the progress meeting.

Celine and Kristina, thanks for sharing your office with me for the last eight months and creating a pleasant working atmosphere for me. I really appreciate your support and encouragements throughout my internship.

I would like to thank my fellow students Alice and Jonathan for the tasty dinners in Leuven and nice conversations we had. A huge thanks to my parents, sister, brother, David, my boyfriend and friends for your continuous support during my education and endless patient.

Abstract

Long-term survival after lung transplantation (LTx) is limited by the development of chronic rejection of which two clinical phenotypes have been defined: bronchiolitis obliterans syndrome (BOS) and restrictive allograft syndrome (RAS). The pathophysiology of chronic rejection remains unclear and consequently prognosis is poor. Therefore, a preclinical model is essential to investigate its elusive pathology. The murine orthotopic LTx in a major antigen-mismatch combination is of greatest clinical relevance since it mimics the procedure of a LTx and recipients require daily immunosuppression. However, until now this model is not used consistently. Hence, the aim is to provide an in-depth investigation of the orthotopic LTx mouse model with a major antigen-mismatch in the context of chronic rejection and its various phenotypes. Innovatively, a longitudinal non-invasive follow-up is implemented using *in vivo* micro-computed tomography (µCT).

In this study, we identified that the murine orthotopic LTx model demonstrated histopathological features comparable to RAS. In addition, µCT scans were regularly taken and showed a progressive worsening graft, with a decreased total lung volume and an increased mean lung density. However, we also observed necrotic lungs and complete consolidation on µCT, indicating a too severe phenotype of chronic rejection. Therefore, the immunosuppressive scheme was adjusted and serial histological assessment was performed at different time points. Initial findings show that this higher immunosuppression and a shorter follow-up period might be better resembling the clinical situation. Nevertheless, the model needs optimization but can become a robust animal model for translational purposes.

Table of contents

List of abbreviations

3D	three-dimensional
ANOVA	analysis of variance
µCT	micro-computed tomography
BAL	broncho-alveolar lavage
BOS	bronchiolitis obliterans syndrome
CLAD	chronic lung allograft dysfunction
CT	computed tomography
DSA	donor-specific antibodies
ECP	extracorporeal photophoresis
FEV_1	forced expiratory volume in 1 second
FVC	forced vital capacity
H&E	hematoxylin and eosin
HU	Hounsfield units
IPF	idiopathic pulmonary fibrosis
ISHLT	International Society for Heart and Lung Transplantation
IVC	individually ventilated cages
IVIS	*in vivo* imaging system
kVp	peak kilovoltage
LTx	lung transplantation
MRI	magnetic resonance imaging
mRNA	messenger ribonucleic acid
OCS	Organ Care System
OB	obliterative bronchiolitis
PA	pulmonary artery
PGD	primary graft dysfunction
POD	post-operative day
PV	pulmonary vein
RAS	restrictive allograft syndrome
SEM	standard error of the mean
TLC	total lung capacity
TLI	total lymphoid irradiation

T_{reg} cells	regulatory T cells
VOI	volume of interest

1. Introduction

Lung transplantation (LTx) is widely accepted as the final treatment option for patients suffering from end-stage pulmonary diseases. Worldwide, approximately 4000 patients receive a LTx every year. According to the registry report of 2017 of the International Society for Heart and Lung Transplantation (ISHLT), chronic obstructive pulmonary disease is the most common indication for an adult LTx (36%), followed by interstitial lung disease (30.3%), cystic fibrosis (15.6%) and pulmonary arterial hypertension (4.4%) (1). Over the last decade, the survival following LTx improved remarkably because of adequate immunosuppression and surgical advancements. Despite these improvements, the survival is still inferior compared to the survival after transplantation of other solid organs, with a mean five year survival of 59% and ten year survival of 41% after LTx (1). This late mortality is mainly due to chronic rejection that occurs in 50% of the patients within five years and accounts for 30% of the mortality between three and five years post-transplant (2). Other known causes of death after LTx are acute rejection, infection, malignancy, cardiovascular or technical problems (1).

1.1 Chronic rejection

Chronic rejection is considered as the recognition of the graft by the recipient as non-self, which elicits an exuberant inflammatory response, leading to progressive graft damage and eventually graft loss. Clinically, chronic rejection is defined as a persistent decline in forced expiratory volume in one second (FEV_1) of at least 20% compared to the two best post-operative values in the absence of other identifiable causes (3). The typical hallmark of chronic rejection was thought to be obliterative bronchiolitis (OB). OB is considered to be the end result of an overt innate and adaptive immune response, causing a fibrotic repair by fibroblasts, which results in remodeling and obliteration of small airways (4). However, diagnosing OB on transbronchial biopsies is complicated given the patchy distribution. Therefore, the term bronchiolitis obliterans syndrome (BOS) is introduced as the clinical correlate of OB. In 2011, however, Sato *et al.* showed that patients with chronic rejection could also suffer from a restrictive pulmonary function defect instead of obstructive and denominated this restrictive allograft syndrome (RAS) (5). This finding demonstrated the heterogeneity within chronic rejection. Therefore, the term chronic lung allograft dysfunction (CLAD) was introduced as an overarching term including all forms of persistent and irreversible declines of FEV_1 (6).

1.1.1 Bronchiolitis obliterans syndrome

Diagnosis, radiology and pathology

BOS is the most frequent phenotype of chronic rejection (60-75%). Diagnosis of BOS is made when a persistent (minimum three weeks) decline in FEV_1 of at least 20% from the average of the two best

values post-transplantation is present, in absence of other identifiable causes (6). Following diagnosis, the median survival is between three and five years (Figure 1A) (3). Other typical hallmarks include air trapping and mosaic attenuation on computed tomography (CT) and OB lesions on pathology (Figure 1 B and D). The former definition is that BOS is an irreversible obstructive small airway disease in which neutrophilic inflammation plays a key role. However, due to new insights in the pathological mechanisms, the definition of BOS is shifting towards a more adaptive immunity-related disease.

Risk factors and mechanism

Many risk factors have been identified for BOS with the main ones being acute rejection, lymphocytic bronchiolitis, infection, primary graft dysfunction (ischemia reperfusion damage), colonization with micro-organisms, presence of donor specific antibodies and air pollution (7).

The pathophysiology of BOS remains largely unclear. However, currently it is thought that repeated injury of the bronchial epithelium causes damage, inducing a repair mechanism. Inflammatory cells are attracted to the airway lesion, infiltrate the lumen and produce cytokines, chemokines and growth factors. In addition, fibroblasts are activated and induce a fibrotic repair. These fibroblasts originate through different ways including proliferation and activation of resident fibroblasts, recruitment of progenitors (fibrocytes) and transition of epithelial and mesothelial cells into mesenchymal cells. Finally, deposition of collagen and extracellular matrix in the airway lumen will result in obstruction of the small airways (8).

Treatment

Several treatment strategies for BOS have been investigated, mostly with limited success. Only azithromycin, a neomacrolide antibiotic, is now being used routinely. This antibiotic reduces airway inflammation and significantly improves the pulmonary function in a subset of BOS patients (9). Extracorporeal photophoresis (ECP) and total lymphoid irradiation (TLI) are immunomodulatory therapies that are tested in BOS patients. Several studies reported an improvement or stabilization of FEV_1 after the addition of ECP or TLI to the standard immunosuppressive therapy (10). Other therapy options are alemtuzumab (anti-CD52) and montelukast (leukotriene receptor antagonist) showing promising results, however, these are only tested in small patient groups (11, 12). In highly selected patients a retransplantation can be a treatment option, although, the survival after a second LTx is inferior compared to the survival after initial transplantation with a three-year survival of 67% (13).

1.1.2 Restrictive allograft syndrome

Diagnosis, radiology and pathology

In 2011, Sato *et al.* demonstrated that 30% of the patients with chronic rejection presented a restrictive pulmonary function defect, denominated RAS (5). The survival post-diagnosis is poor with only six to

18 months median survival (Figure 1A) (3). Currently, there is no internationally accepted definition for RAS, therefore several groups have used different diagnostic criteria to define restriction. Sato initially defined RAS as an irreversible decline in total lung capacity (TLC) of at least 10% in combination with 20% decline in FEV_1 compared to the two best values after transplantation. Since TLC measurements are expensive, time consuming and not routinely performed as part of the follow-up in every center, Todd *et al.* used a decrease in forced vital capacity (FVC) of ≥ 20% to diagnose RAS (14). Verleden *et al.* additionally used $FEV_1/FVC > 0.7$ (15). Later, it became clear that these patients showed similar persistent pleuroparenchymal infiltrates on CT scans. Therefore Suhling proposed to add the presence of pulmonary infiltrates on CT to the definition of RAS (16). In addition to pleuroparenchymal infiltrates, (sub)pleural thickening, substantial parenchymal fibrosis, bronchiectasis (bronchial dilatation) and reticulations are seen on CT images of RAS lungs compared to BOS and healthy lungs (Figure 1C). Histological examination of RAS lungs shows pleuroparenchymal fibro-elastosis (17). This is defined by visceral pleural fibrosis associated with subpleural, intra-alveolar fibrotic changes consisting of a mixture of elastic and fibrous tissue (Figure 1E). However, also other patterns are found in RAS lungs, including nonspecific interstitial pneumonia and fibrosis-induced subpleura or paraseptal emphysema, demonstrating a histomorphological spectrum within the disease (18). Furthermore, OB lesions are often identified. Both on histology and CT images a sharp demarcation can be present between healthy and diseased zones (19).

Risk factors and mechanism

Almost all risk factors applicable to BOS are associated with RAS including infection, acute rejection, lymphocytic bronchiolitis, colonization with *P. aeruginosa* and elevated neutrophilia in broncho-alveolar lavage (BAL) fluid (20). Currently, the pathophysiological mechanisms underlying RAS are mostly elusive. However, recent evidence demonstrated that humoral immunity might be involved in the pathogenesis of RAS demonstrated by lymphoid cell organization exclusively found in RAS lungs (21) and increased immunoglobulins in BAL of RAS patients compared to control and BOS patients (22). Moreover, the presence of persistent donor specific antibodies (DSA) is associated with a higher risk for RAS development (23). These findings support the idea that RAS is the consequence of an excessive adaptive immune response directed towards the non-self graft, mainly mediated by humoral immunity. However, the innate immunity also seems to be important in RAS as eosinophils and macrophages were upregulated in RAS lungs compared to control and BOS (21). More research will be necessary to reveal the underlying mechanisms.

Treatment

Similar to BOS, treatment of RAS patients remains difficult. The same therapy options for BOS have been tested in RAS, unfortunately with limited success. Given the presence of extended fibrosis in RAS,

anti-fibrotic treatments used in idiopathic pulmonary fibrosis (IPF) have been tried in patients with RAS. Examples are pirfenidone (24) and nintedanib (25), which showed stabilization of the disease after treatment in case reports. A retransplantation could be considered, however, only in well-selected patients since the three-year survival after retransplantation is only 33% in patients with RAS and within survivors, there was a high rate of patients redeveloping chronic rejection (13). Currently, an effective treatment for BOS and RAS is still lacking. A better understanding of the pathology of chronic rejection can help in the development of new therapeutic strategies.

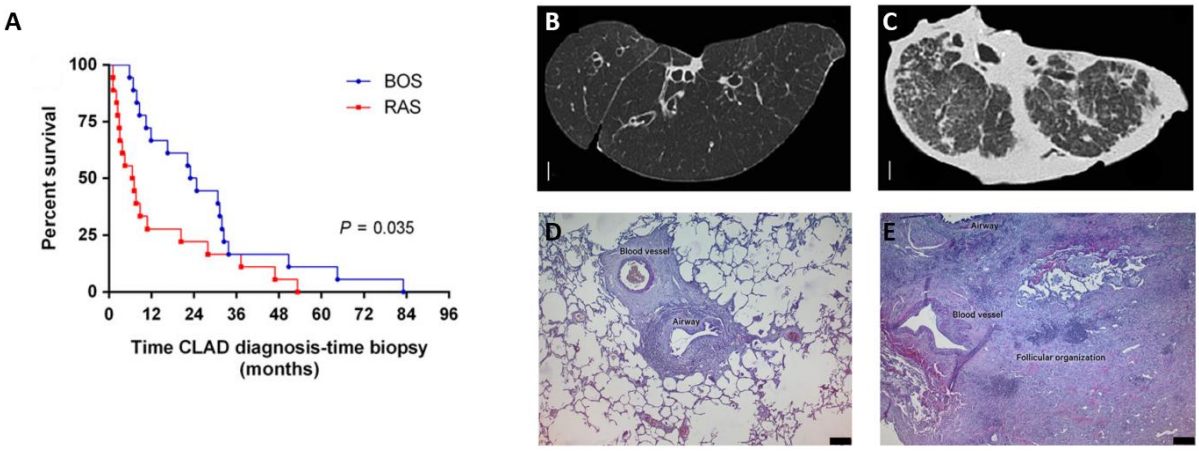

Figure 1: Mortality rate of BOS and RAS at time of diagnosis (A). Representative images of BOS (B and D) and RAS (C and E). *(A) Kaplan-Meier survival curve presenting mortality rate of BOS and RAS between diagnosis and death (21). (B) and (C) are CT images of frozen explant lungs (26), (D) and (E) the corresponding typical histological features (21). Overall, the parenchyma in BOS lungs looks normal with narrowed fibrotic airways on histology, while thickened pleura and fibrosis are observed in RAS lungs. RAS is characterized by intensive fibrosis in parenchyma, blood vessel and airways with follicular organization. Scale bar of CT scans indicate 1 cm, scale bar of histological images indicate 200 µm. BOS: bronchiolitis obliterans syndrome; RAS: restrictive allograft syndrome; CLAD: chronic lung allograft dysfunction.*

1.1.3 Animal models

The use of animal models is one of the best ways to elucidate underlying pathophysiologic mechanisms of various diseases and to discover potential new therapeutic strategies. Several animal models to study chronic rejection have been used.

Tracheal transplant models

The most widely used model to study rejection after LTx is the heterotopic tracheal transplant model (Figure 2A). This model consists of the subcutaneous implantation of a donor trachea on the back or in the omentum of a genetically different rat or mouse (allograft). The strength of this model is that the allografts develop OB-like lesions with obliteration of the tracheal lumen within 28 days, which are not seen in isografts (transplantation in genetically identical animals) (27). The additional advantages of this model are the reproducibility, the simple surgical techniques and the ability to produce a large number of transplanted animals in a relatively short period. However, one has to acknowledge the

limitations as well, as the graft is not perfused or ventilated. Moreover, the anatomy of the trachea is different since it is a large cartilaginous airway, while human OB develops only in small airways. Therefore, the heterotopic tracheal transplant model can be used as a first indication of allo-immunity induced obstruction of airways, but does not reflect chronic rejection of the lung as seen in humans. Some of the limitations of this model can be overcome by using the heterotopic intrapulmonary tracheal transplant model (Figure 2B). In this model, the trachea is directly implanted into the pulmonary parenchyma of the lung. It still has the simplicity and reproducibility of the heterotopic tracheal transplant model, but here the trachea is placed in a more relevant pulmonary environment (28). Nevertheless, this model still lacks connection with ambient air. Therefore, an orthotopic tracheal transplant model has been developed, in which an anastomosis is performed between the tracheas (Figure 2C) (29). After the tracheal transplantation, epithelial cells from the donor trachea are damaged, while recipient-derived epithelial cells will migrate to the donor trachea and replace the epithelial lining. In this way the airway lumen stays open with moderate subepithelial fibrosis (30).

Orthotopic single-lung transplant model

Considering the disadvantages of the heterotopic and orthotopic tracheal transplant models, an orthotopic single-lung transplant model was introduced (Figure 2D). It mimics the surgical procedure of a human LTx more closely, with a graft that is vascularized and ventilated. The orthotopic LTx has first been developed in large animals including dogs, swine and primates (31-33). Given that large animals are very expensive, difficult to house and to handle, other animals were tested. In ferrets, orthotopic left lower lobe transplantation was established and developed the entire spectrum of human histopathological lesions including acute rejection, lymphocytic bronchiolitis and obliterated airways (34). However, ferrets are not commonly used laboratory animals and is therefore an inferior model. Orthotopic single left LTx is also described in rats and showed promising results, however the lack of transgenic and knock-out strains is a disadvantage of using rats (35). Considering the above findings, the most relevant species is the mouse, although their small size makes the surgery a big challenge (36). First, this model was established in mice to investigate ischemia reperfusion damage and acute rejection. Balb/c mice served as donor and C57BL/6 as recipients. These transplanted mice developed very severe acute rejection within seven days post-transplant which completely destroyed the lung, making a longer follow-up to examine chronic rejection impossible (37). A solution for this problem came from Fan *et al.*, by transplanting mice with a minor antigen-mismatch (C57BL10 → C57BL/6), developing only mild rejection after one week and mice could be investigated for a longer time. However, they demonstrated OB-like lesions in only 50% of all mice at 21, 28 and 35 days after transplantation (38). One should pay attention to the difference in airway structure between human and mouse since mice lack small airways and BOS is a small airway disease (39). In 2012, our research

group developed a major antigen-mismatch model (Balb/c → C57BL/6) with daily immunosuppressive treatment (cyclosporine + steroids) with a follow-up of ten weeks. This model resembles the human situation, but only 25% to 50% of the allografts showed airway obliteration (40). After the clinical identification of the chronic rejection phenotypes, the various strain combinations were compared in the context of chronic airway fibrosis. The major mismatch model showed bronchovascular fibrosis and inflammation, pleural and septal thickening and parenchymal inflammation on histology of the allografts, compatible with the histological presentation in human RAS lungs (41, 42). The strength of the model is the close proximity to the human situation since human LTx is performed between major mismatched individuals and patients need daily immunosuppression (43).

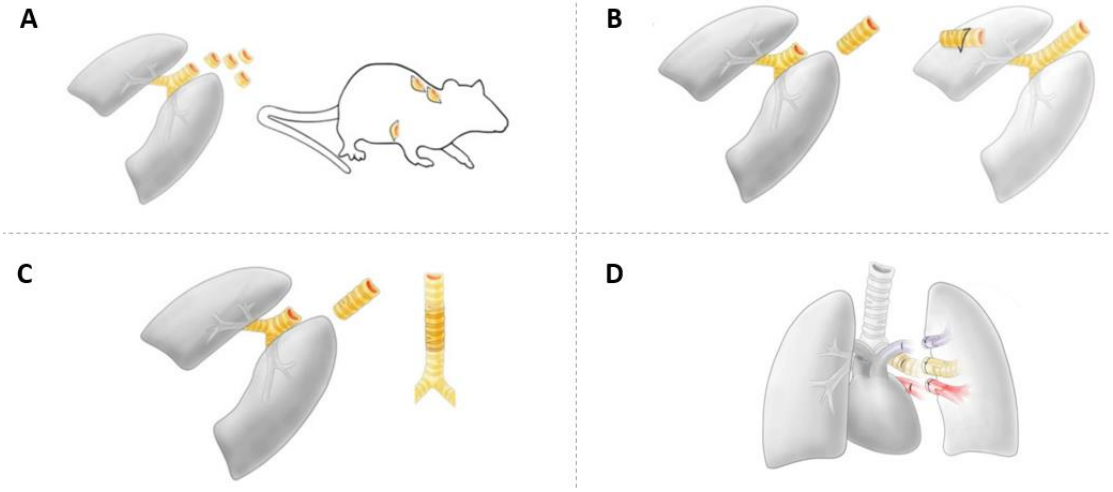

Figure 2: Animal models of chronic rejection. (A) Subcutaneous heterotopic tracheal transplantation. (B) Intrapulmonary heterotopic tracheal transplantation. (C) Orthotopic tracheal transplantation. (D) Orthotopic single-lung transplantation (44).

Assessment of orthotopic single-lung transplant model

Currently, the assessment of disease severity of the orthotopic LTx model is primarily based on end-stage procedures including macroscopic examination, histopathology and mRNA expression levels. Measurement of arterial blood gases and BAL can only be performed right before sacrifice. In this way only a snapshot is examined of the situation at that time, hence precluding dynamic evaluation of disease progression. To circumvent this problem, serial sacrifice and thus evaluation of transplanted animals at different time points can be a solution (40). However, this is not the same as a longitudinal follow-up of individual mice. Repeated pulmonary function measurements could be used to evaluate the function of the lung over time but our group reported that this is not a good tool to diagnose and evaluate chronic rejection in mice (40). *In vivo* imaging of mouse lungs with micro-computed tomography (µCT) becomes increasingly interesting in this field. µCT is a three-dimensional (3D) x-ray imaging method providing high resolution and excellent air-tissue contrast, yielding visual and quantitative information of the whole lung (45). Scanning is used in a longitudinal fashion to evaluate disease progression and therapy effects in various animal models of lung disease including cancer,

fibrosis, emphysema and ischemia reperfusion damage after LTx (46-48). De Langhe *et al.* developed a non-invasive, dynamic *in vivo* µCT protocol for lung imaging in mouse models of lung fibrosis and emphysema. By applying respiratory gating during the scan, moving artefacts caused by respiration are significantly reduced, resulting in high quality images. Using this protocol, they were able to quantify dynamic changes in pulmonary pathology (47). Later, these quantitative measurements, such as lung volume and mean lung density, were validated as biomarkers in preclinical models of lung fibrosis and fungal lung infections (45). The ability of quantifying µCT images makes it very interesting for the longitudinal follow-up after the orthotopic single LTx.

2. Hypotheses and goals

There are three specific goals of this thesis.

2.1 The relationship between the murine lung transplant model and chronic rejection phenotypes

Given the recent discovery of the different phenotypes of chronic rejection, being BOS and RAS, it is necessary to revise the major mismatched murine orthotopic LTx model to establish which phenotype the model reflects. Based on previous experiments, **we hypothesize that the major antigen-mismatch orthotopic LTx mouse model mimics RAS.**

2.2 Longitudinal follow-up in the murine lung transplant model using *in vivo* µCT

End-stage disease only delivers limited insight into disease pathophysiology, hence longitudinal follow-up is needed to gain knowledge about the disease progression. Therefore, **we hypothesize that *in vivo* µCT can be a useful tool to evaluate the progression of chronic rejection within the major mismatched murine orthotopic LTx model.** To examine the use of µCT in this model, multiple scans were performed during follow-up and lung volume and density were both quantitatively measured.

2.3 The correlation between µCT and histology

Since *in vivo* µCT scanning can be used in a longitudinal fashion without sacrifice of the transplanted animals in contrast to histopathological analysis, we aim to investigate the correlation between *in vivo* µCT and histology. In addition, *ex vivo* µCT of the explanted lungs can yield higher resolution than *in vivo* µCT, therefore the goal is to correlate *ex vivo* µCT with corresponding histology. **The hypothesis is that µCT analysis correlates closely with histopathological examination.**

3. Materials and methods

3.1 Animals

All animals received human care in compliance with "The Principles of Laboratory Animal Care" formulated by the National Society for Medical Research and the "Guide for the Care and Use of Laboratory Animals" published by the National Institutes of Health (49). The experimental procedure was approved by the Ethical Committee for Animal Research at KU Leuven. All animals were purchased from Janvier Labs (Le Genest Saint Isle, France) at eight weeks of age (20 to 25 grams). C57BL/6N (H-2K^{b}) male mice, 25-30 gr, were used as recipients and as donors for isografts. Male Balb/c (H-2K^{d}) mice served as donors for allografts. After surgery, all mice were housed in a conventional facility with individually ventilated cages (IVC).

3.2 Orthotopic single-lung transplantation

The recipient procedure was performed by a trained PhD student (T. Heigl) of the host lab. An operating microscope (Zeiss, Zaventem, Belgium) with 4 – 24x magnification was used for both donor and recipient procedures.

3.2.1 Donor procedure

Donor mice were anesthetized with a mixture of xylazine (100 mg/kg) and ketamine (10 mg/kg) administered by an intraperitoneal injection. A tracheostomy was performed and the mouse was connected to a ventilator (MiniVent type 845, March-Hugstetten, Germany) with a 20-gauge catheter. The abdomen and thorax were opened and 100 µL of heparin (LEO Pharma, Ballerup, Denemarken) was injected directly into the right lobe of the liver. Afterwards the lungs were flushed with 5 mL Organ Care System (OCS) Lung Solution (HealthLink, Hertogenbosh, The Netherlands) through the right ventricle. Subsequently, the heart-lung block was excised with inflated lungs.

3.2.2 Graft preparation

The donor left lung was isolated and the hilum was prepared for cuffing (Figure 3A). The cuff of the pulmonary artery was made of a 26-gauge Teflon catheter (BD, Erembodegem, Belgium), the bronchus cuff of a 20-gauge catheter and pulmonary vein cuff of a 22-gauge catheter (Figure 3B). The pulmonary artery was passed through the cuff and folded over the cuff exposing the endothelial surface (Figure 3C) and secured with a 10-0 nylon ligature (Ethicon, Lidingö, Sweden). The bronchus and pulmonary vein were cuffed in analogous fashion. The cuffed left lung was placed in OCS preservation solution at 4°C until implantation (Figure 3D).

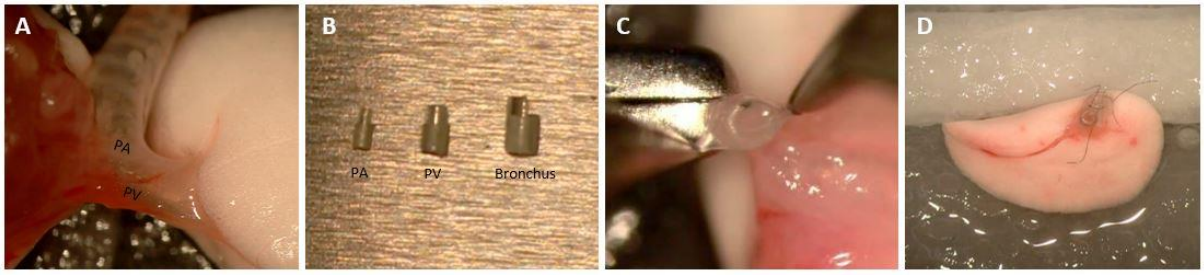

Figure 3: Donor procedure. *(A) After excising the heart-lung block, the hilum of the left lung was exposed and dissected. (B) The cuffs were adjusted for the size of the structure. (C) The pulmonary artery is folded over the cuff and secured by a 10-0 nylon ligature. Bronchus and pulmonary vein were cuffed in the same manner. (D) Afterwards, the cuffed left lung was placed in an OCS preservation solution at 4°C. PA: pulmonary artery; PV: pulmonary vein; OCS: Organ Care System.*

3.2.3 Recipient procedure

The recipient animal was anesthetized with isoflurane (Iso-Vet, Dechra, Belgium) in an induction box. The mouse was intubated and connected to the ventilator (UNO microventilator, Zevenaar, The Netherlands). The animals were maintained under general anesthesia with a mixture of 50% air, 50% oxygen and 2.5% isoflurane. The left chest wall was shaved and sterilized, a left thoracotomy was performed through the third intercostal space. The left native lung was retracted laterally by placing a clamp to expose the hilum (Figure 4A). The hilum was dissected to separate the pulmonary artery, pulmonary vein and bronchus from each other. The pulmonary artery and vein were occluded with a slipknot (10-0 nylon ligature) proximally to the heart (Figure 4B). First, the vein was anastomosed by making a small transverse incision into the anterior wall of the vein (Figure 4C). Afterwards, the cuffed vein from donor lung was inserted and secured with a 10-0 ligature (Figure 4D). Both bronchus and artery were inserted and secured in the same way (Figure 4E). The transplanted lung was reperfused by releasing the slipknots of the vascular structures (Figure 4F). Hereafter, the chest was closed in two layers and the recipient mouse was extubated. Pain medication with buprenorphine (0.1 mg/kg) was given every eight hours during three days after surgery.

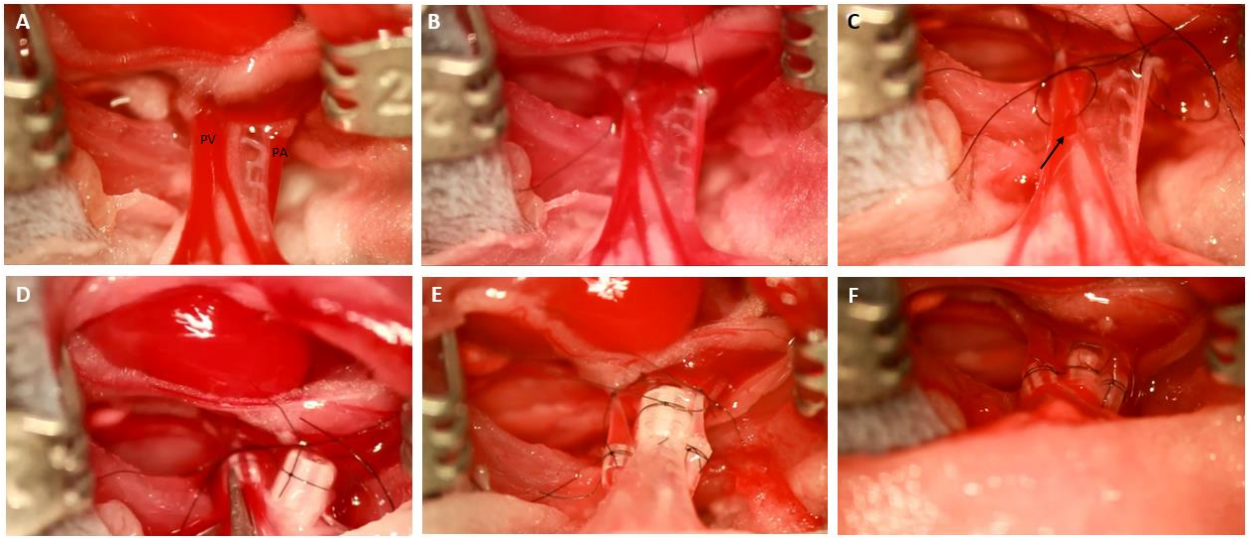

Figure 4: Recipient procedure. *(A)The recipient left lung was retracted and the hilum was exposed. (B) Pulmonary artery and vein were occluded. (C) A small transverse incision was made in the pulmonary vein indicated by black arrow. (D) The cuffed donor pulmonary vein was inserted into the recipient pulmonary vein and secured with a 10-0 nylon ligature. (E) The same was done for bronchus and pulmonary artery. (F)The lung was reperfused and placed back in the chest. PA: pulmonary artery; PV: pulmonary vein.*

3.2.4 Immunosuppressive treatment

The normal immunosuppressive scheme consisted of 10 mg/kg/day cyclosporine (Sandimmun®, Novartis, Vilvoorde, Belgium) and 1.0 mg/kg/day methylprednisolone (SoluMedrol®, Pfizer, Brussels, Belgium) daily administered subcutaneously until sacrifice.

3.3 Study design

The study design is illustrated in Figure 5. This project includes an isograft (n = 8) and allograft (n = 8) group. These animals received daily immunosuppression and at POD 7, 35 and 70 *in vivo* µCT scans were performed. After the last µCT scan, mice were sacrificed and explant specimen were used for histopathological analysis or an additional *ex vivo* µCT was taken. In addition, serum level of cyclosporine was measured by a clinical laboratory at week eight in isografts and allografts (Sequential enzyme immunoassay, Dimension® RXL, Siemens Medical solutions, Diamond diagnostics, USA).

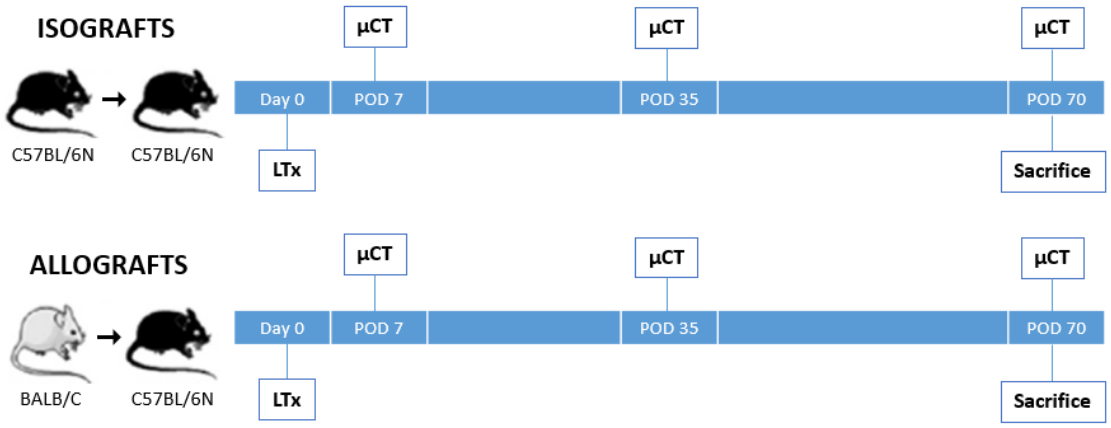

Figure 5: Study design. *Isografts: left LTx from C57BL/6N mouse to C57BL/6N mouse. Allografts: left LTx from Balb/c mouse to C57BL/6N mouse. LTx: lung transplantation; POD: post-operative day.*

3.4 *In vivo* µCT imaging

All µCT imaging was performed on a small animal µCT scanner (SkyScan 1278, Bruker microCT, Kontich, Belgium). Mice were anesthetized with isoflurane and placed in supine position on the scanner bed, anesthesia was maintained during the scan with 2% isoflurane in 100% oxygen by a nose cone. Respiratory-gated µCT images of free-breathing animals were acquired by recording thoracic breathing movements with a visual camera, detecting the up- and downward movement of the thorax (Figure 6). The complete respiratory cycle was divided into four phases, from the initiation of inspiration to end-expiration. After scanning, all images were sorted in the corresponding phase of respiration in

which they were acquired. Scan parameters were 55 kVp X-ray source voltage combined with a 0.5 mm aluminum filter, 300 µA source current, 120 ms exposure time per projection, acquiring ten projections per position with 0.4° increments over a total angle of 180°. This resulted in a scanning time of 23 minutes yielding four reconstructed 3D datasets with a voxel size of 54.6 μm^3 corresponding to four different phases of the breathing cycle. The images were reconstructed using NRecon software (version 1.7.0.4, Bruker microCT) with following parameters: smoothing of one, beam-hardening correction of 10%, post-alignment and ring artefact reduction were optimally set for each individual scan. The images were calibrated to Hounsfield units (HU) via measurements of a scanned phantom consisting of an air-filled 1.5 mL tube inside a water-filled 50 mL tube. The mean gray scale index of water (122.2376) was set to zero HU and the mean gray scale index of air (6.08375) to -1000 HU. Based on HU, the density was converted to gram/liter.

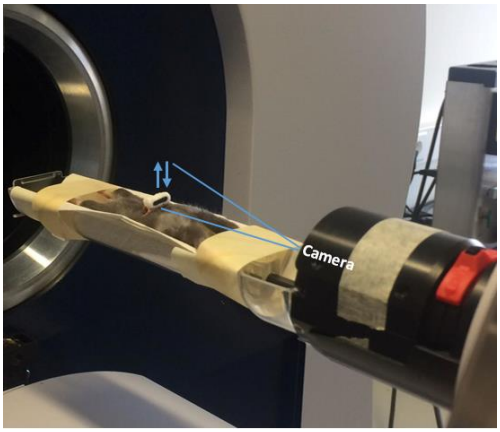

Figure 6: µCT imaging set-up. *The visual camera inside the µCT machine detects up- and downward movement of the marker attached to the thorax.*

3.4.1 *In vivo* µCT image analysis and quantification

Image analysis and quantification were performed using software provided by the manufacturer (CTAn, version 1.16.8.0 +, Bruker microCT). Segmentation and quantification of lung volumes were performed using a custom written automated algorithm that was applied to all datasets as defined, validated and described previously (47). This algorithm is based on a selected threshold (-234.5165 HU) which excludes all pixels with densities above this value resulting in automatic segmentation of pixels with a density corresponding to air, in this way aerated lung volume is measured (Figure 7). Quantification of total lung volume and mean lung density was performed for a manually delineated volume of interest (VOI) on the transversal µCT images at end-expiration. Lung tissue (non-aerated) volume was calculated as the total lung volume (manually delineated) minus the aerated lung volume (automatically derived). In addition to using this algorithm, 3D image reconstruction was performed using CTVol software (version 2.3.2.0, Bruker microCT). In order to compare the data, a baseline was created by scanning and quantifying four healthy C57BL/6N mice and four healthy Balb/c mice.

Figure 7: Qualitative and quantitative assessment of lung volume and density by in vivo µCT. *The crucial steps of the automated algorithm to quantify lung volume and density showed in an isograft. Pixels with grayscale below -234.5165 Hounsfield Units (HU) were selected, segmenting air-containing pixels. Afterwards, a 3D reconstruction was made that visualized the aerated lung volumes.*

3.5 *Ex vivo* µCT imaging

To perform an *ex vivo* µCT, the heart-lung block was air-inflated to total lung capacity and frozen solid in the fumes of liquid nitrogen. Whole lungs were scanned with a µCT scanner with a cooling stage (-30°C) (SkyScan 1172, Bruker microCT). Scan parameters were 40 kVp source voltage, 226 µA source current, no filter was used, 295 ms exposure time, four frames per position with 0.3° rotation step. This protocol resulted in 30 minutes scanning time and a voxel size of 13.9 μm^3. Reconstruction of the images was performed using NRecon, parameters were smoothing of two, beam-hardening reduction of 30%, post-alignment and ring artefact reduction were optimally set for each individual scan. Four allografts and four isografts were *ex vivo* scanned, the remaining were directly fixed and embedded as described below.

3.6 Histology

The heart-lung block was excised and fixed in 4% paraformaldehyde before paraffin embedding for histology. The frozen lungs used for *ex vivo* µCT were fixed in 4% paraformaldehyde in acetone after scanning and embedded in paraffin. Five µm thick sagittal sections were cut with a microtome (Microm HM360 Microtome, Thermo Fisher Scientific, Asse, Belgium). Sections were stained with hematoxylin and eosin and evaluated by an experienced lung transplant pathologist (Prof. dr. Erik Verbeken). A Masson-Trichrome staining was performed to visualize the degree of fibrosis.

3.7 Statistical analysis

GraphPad Prism version 6.01 (GraphPad Software, San Diego, California, USA) was used for statistical analysis. Results are presented as mean ± SEM. To compare between isografts and allografts for start weight, cyclosporine serum levels and between initial allograft group and allograft group with higher immunosuppression for volume and density measurements at POD 7 or POD 35, normality was checked with Shapiro-Wilk and subsequently an appropriate unpaired T-test was performed.

Difference in weight evolution between isografts and allografts was tested with two-way analysis of variance (ANOVA). The difference in distribution of normal grafts and consolidated grafts on *in vivo* µCT was compared using Chi-squared test. Differences in lung volume and mean lung density were evaluated with Friedman test in combination with a Dunn's *post hoc* test. Baseline comparisons concerning volume and density were performed with Kruskall-Wallis ANOVA and Dunn's *post hoc* test. A p-value of < 0.05 was considered significant.

4. Results

4.1 The major antigen-mismatch orthotopic single-lung transplant mouse model in the context of the phenotypes of chronic rejection

Recently the different manifestations of chronic rejection were discovered, including BOS and RAS. This led to the re-investigation how chronic rejection manifests in the orthotopic single-lung transplant model using histopathology.

4.1.1 Survival and general health

Of the mice that were successfully operated (surviving more than 24 hours), all mice survived except one allograft that died after two days due to a pneumothorax. Weight evolution in isograft and allograft groups is illustrated in Figure 8. There was no difference in start weight in both groups, allografts had a start weight of 27.29 g (25 – 29.5) and isografts of 27.26 g (25.9 – 28.6) ($p = 0.97$). No significant differences were observed between isograft and allograft group in weight evolution ($p = 0.88$) (Figure 8).

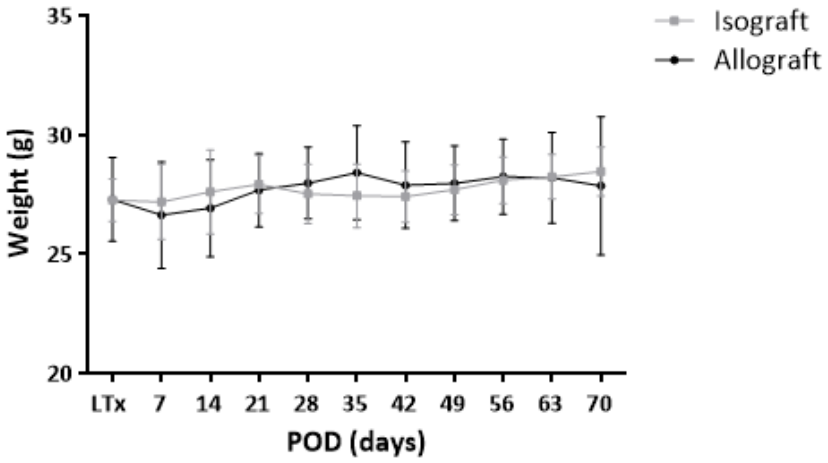

Figure 8: Weight evolution of isografts and allografts. *LTx: lung transplantation; POD: post-operative day. Error bars indicate SEM of replicate samples, n = 8 in both groups.*

4.1.2 Macroscopic evaluation

Macroscopic examination of the transplanted isograft lungs showed normal lung morphology (n = 7) (Figure 9A). One isograft presented yellow and was attached to the chest. In the allograft group, morphological differences were observed including dense reddish lungs resembling fibrosis and inflammation (n = 3) (Figure 9B), some appeared dark yellow and shrunken (n = 2) (Figure 9C), others showed severe adhesions to the chest wall (n = 3) (Figure 9D).

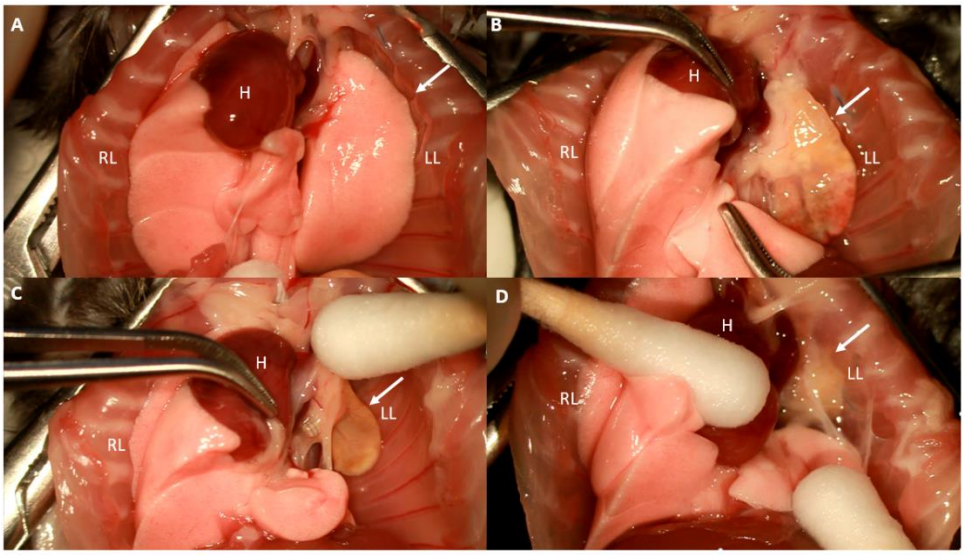

Figure 9: Macroscopic pictures of isograft and allografts. *(A) Transplanted lungs of isografts showed normal macroscopic lung tissue. Allografts showed severe morphological changes including a dense reddish lung (B), dark yellow and shrunken lung tissue (C) and completely attached to chest wall (D). Left lungs are indicated by an arrow. RL: right lung; H: heart; LL: left lung.*

4.1.3 Histology

Transplanted lungs of isografts and native right lungs of allografts showed normal lung parenchyma ten weeks post LTx (Figure 10). In the allograft group, two mice were excluded: one mouse demonstrated total necrosis probably due to anastomosis problems following surgery. The other showed grossly normal lung tissue, however severe lymphocytic giant cell infiltration was found resembling a post-transplant lymphoma. The other six allografts showed a variety of changes of the graft (Figure 11). One mouse demonstrated pathology similar to RAS including fibrosis, inflammation, obstructed airways, thickened pleura and lymphoid follicles (Figure 11) (Figure 22S). There was one animal showing (sub)pleural fibrosis, alveolar fibrosis, necrotic areas and some normal alveoli, representing an intermediate stage (Figure 11). Three mice showed encapsulation of the lung and many cell nuclei without recognizable native lung structure resembling complete necrosis (Figure 11). Given that only one animal showed relevant lesions, while the others showed too extensive lung pathology, we conclude that the rejection seems to be too severe.

4.1.4 Cyclosporine serum levels

Serum levels of cyclosporine were assessed in both groups at week eight. There was no difference between the median serum level of isografts (662 µg/L) and allografts (596.5 µg/L) ($p = 0.85$). In addition, no association was found between cyclosporine serum levels and necrotic or RAS-like allografts.

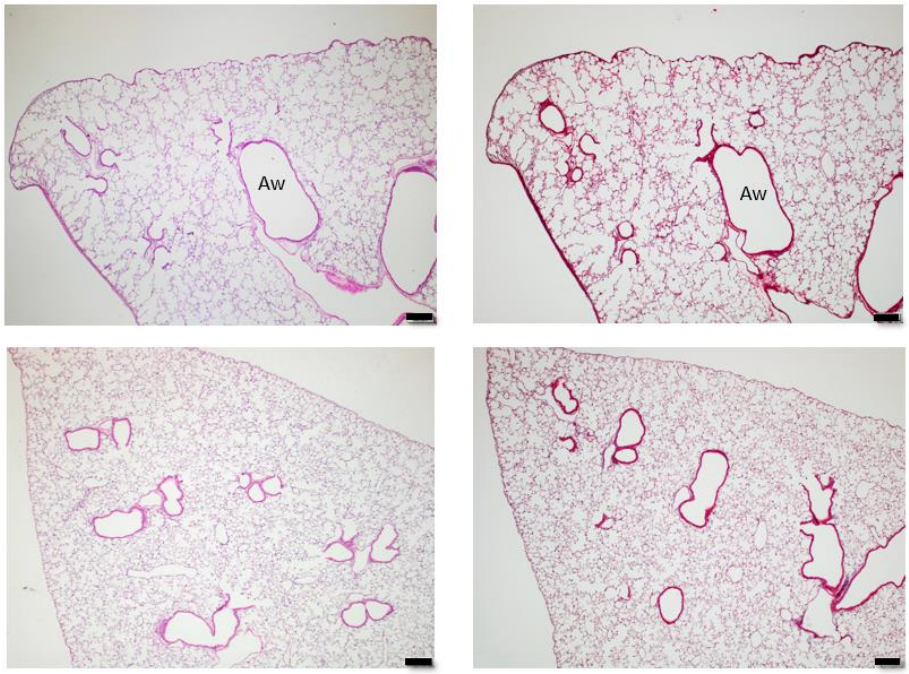

Figure 10: Histology of isograft LTx lung (upper) and native right lung of allograft (lower) 70 days after LTx. *H&E staining (left) and Masson-Trichrome staining (right) showed normal histology. Scale bars indicate 200 µm. H&E: hematoxylin and eosin; LTx: lung transplantation. Aw: airway.*

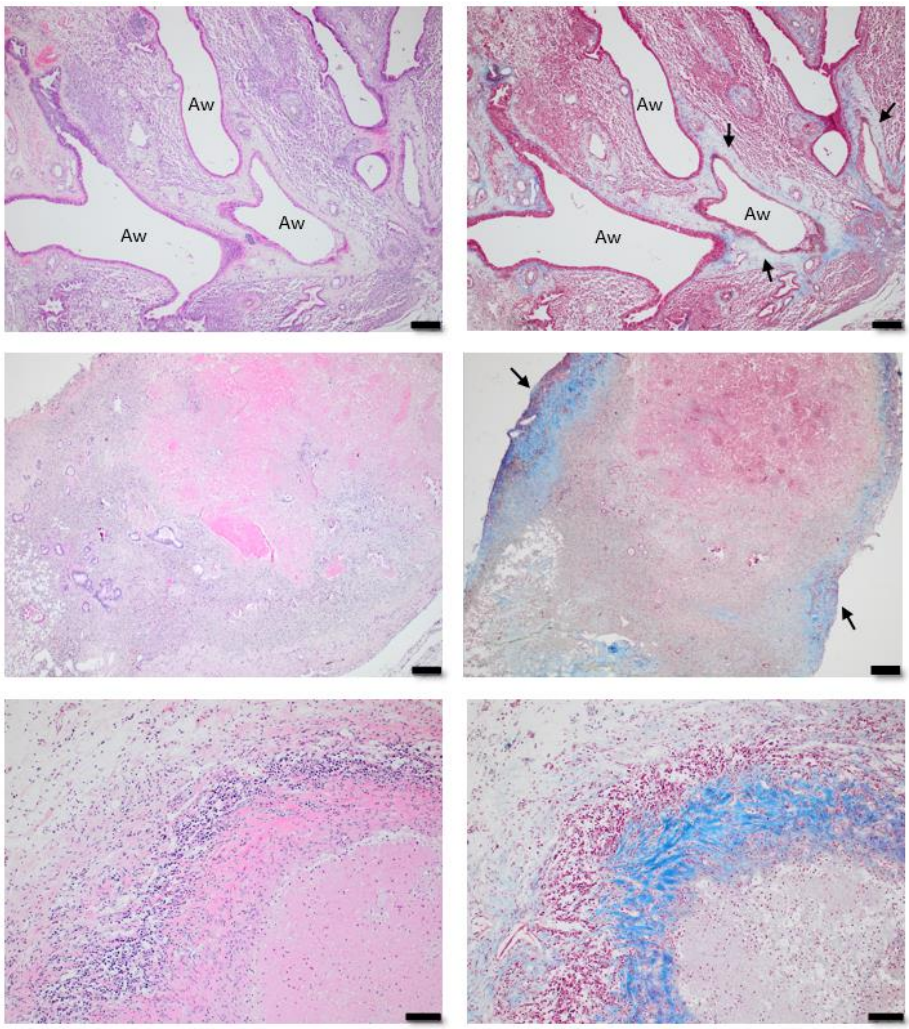

Figure 11: Representative images of H&E and Masson-Trichrome staining of allograft LTx lungs. *Severe RAS-like pattern (top). Arrows on Masson-Trichrome indicate fibrotic regions. Fibrosis, necrosis, normal tissue (middle). Arrows on Masson-Trichrome indicate (sub) pleural fibrosis. Complete necrosis (bottom). Scale bars of upper four images indicate 200 µm. Scale bar of lower two images indicate 100 µm. H&E: hematoxylin and eosin; LTx: lung transplantation; Aw: airway.*

4.2 Longitudinal follow-up of the murine lung transplant model using *in vivo* µCT

4.2.1 Visual assessment of *in vivo* µCT

In vivo µCT imaging can be used for longitudinal follow-up of chronic rejection in mice. To evaluate the disease progression in the orthotopic LTx mouse model, µCT scans were performed at POD 7, 35 and 70 in isografts and allografts. Representative images of µCT scans and 3D reconstruction are shown in Figure 12.

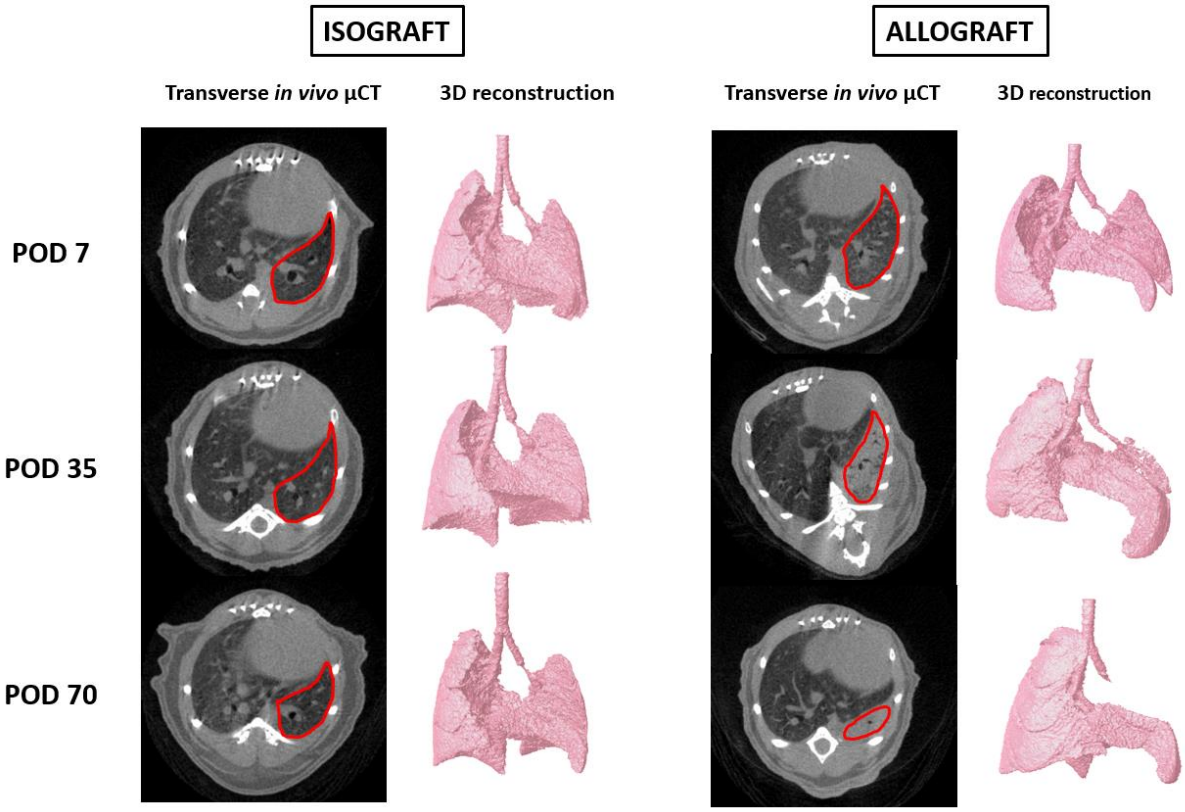

Figure 12: Longitudinal in vivo µCT of allograft and isograft groups. *Representative images of transversal µCT and respective 3D reconstructions of aerated lung tissue at POD 7, 35 and 70 at end-expiration. The left transplanted lung is delineated in red. POD: post-operative day.*

Table 1 provides an overview of the direct observations of µCT images of the transplanted lungs in allografts and isografts at POD 7, 35 and 70. µCT scan of isografts at POD 7 showed normal appearing lungs in four animals, while the others were consolidated as the lung could not be differentiated from the surrounding tissue and chest wall. However, the transplanted lungs recovered as scans at POD 35 and 70 were all showing normal lungs except one, which probably had an infection. Allograft lungs appeared normal on POD 7 in two animals. In the remaining six animals, the transplanted lung was consolidated. At POD 35, one allograft showed a dens transplanted lung. The other seven mice

demonstrated complete consolidation, in some cases white spots were observed, indicating hyperdense areas. The last scan revealed total consolidation in all allografts.

Table 1: Overview of observations of µCT scans of transplanted lungs in allografts and isografts. *Consolidation means that the lung could not be distinguished from the surrounding soft tissue and chest wall. Bold p-values indicate significance. POD: post-operative day.*

	Isografts		***Allografts***		***p-value***
POD 7	4 normal	4 consolidation	2 normal	6 consolidation	0.30
POD 35	7 normal	1 consolidation	1 dense	7 consolidation	**0.0027**
POD 70	7 normal	1 consolidation	0 normal	8 consolidation	**0.0004**

4.2.2 Quantification of lung volume and density

Quantification of total lung volume and mean lung density was performed for both native right lungs and transplanted left lungs in isografts and allografts. Total lung volume of native lung of isografts was stable over time ($p = 0.64$), while allografts native total lung volume significantly increased during follow-up ($p = 0.032$) (Figure 13A). The increase in native lung volume in allografts is mainly due to an enlargement of the aerated lung tissue (Figure 23S). Total native lung volume in both isografts at POD 7 ($p = 0.039$) and allografts at POD 70 ($p = 0.013$) were higher compared to baseline (POD 0) (Figure 13A). Isografts transplanted lungs seemed to increase from POD 7 to POD 35 and remained stable afterwards ($p = 0.16$) (Figure 13B). The lung volume of the transplanted lung in the allograft group decreased ($p = 0.015$) (Figure 13B), which was predominantly caused by a decrease in aerated lung tissue (Figure 24S). The Balb/c baseline (POD 0) was significantly higher in comparison with transplanted allograft lungs ($p = 0.0015$) (Figure 13B). The transplanted lungs from isografts were approximately the same as the baseline of C57BL/6N (POD 0) (Figure 13B).

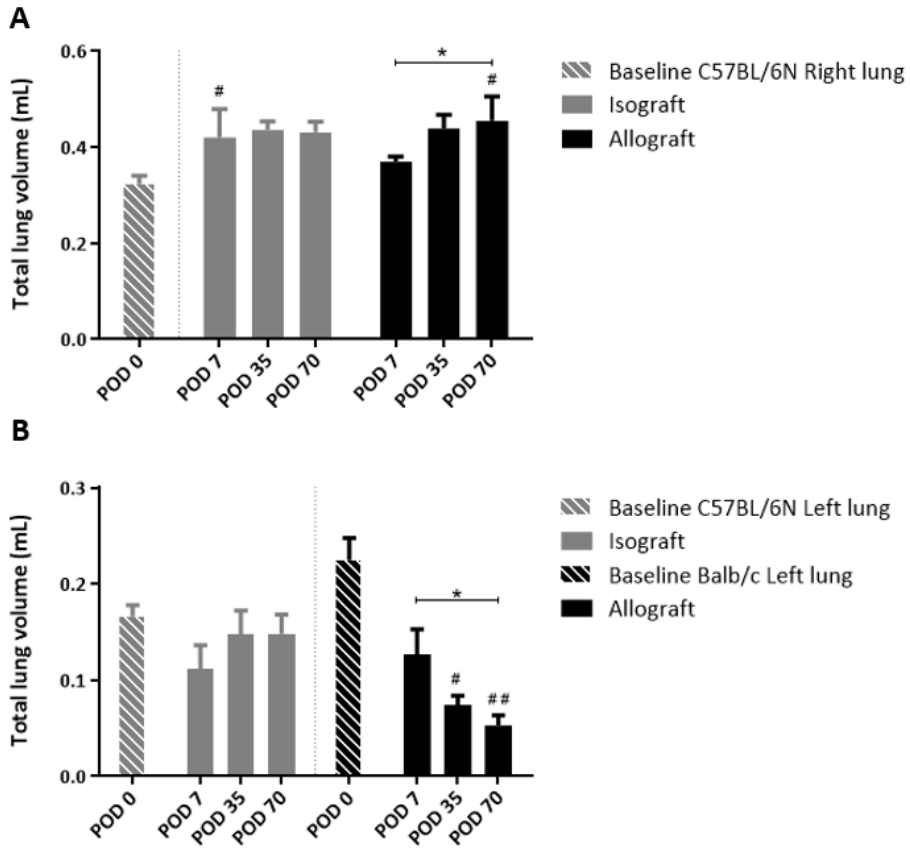

Figure 13: Total lung volume evolution in allograft and isograft groups at POD 0, 7, 35 and 70. *(A) Graph of total lung volume of native right lungs. (B) Graph of total lung volume of transplanted left lungs. Volumes were calculated based on end-expiratory µCT images. POD: post-operative day. Error bars indicate SEM of replicate samples, n = 8 (POD 0: n = 4). * p < 0.05; ** p < 0.01; # p < 0.05 compared with corresponding baseline; ## < 0.01 compared with corresponding baseline.*

Mean lung density is measured based on gray values of the images, later converted to gram/liter. The mean lung density of native lungs was stable for both isografts (p = 0.42) and allografts (p = 0.65) during follow-up (Figure 14A). The baseline (POD 0) of native right lungs was also comparable to the densities of both groups (Figure 14A). In the isograft group, density of the transplanted lung first seemed to decrease from POD 7 to POD 35, thereafter the mean lung density remained similar (p = 0.42) (Figure 14B). Baseline (POD 0) showed equal density of healthy C57BL/6N mice and isografts (Figure 14B). The mean lung density of transplanted lungs of allografts, however, increased significantly over time (p = 0.015) (Figure 14B). In addition, mean lung density at POD 70 was significantly denser compared to baseline of Balb/c mice (POD 0) (p = 0.0007) (Figure 14B).

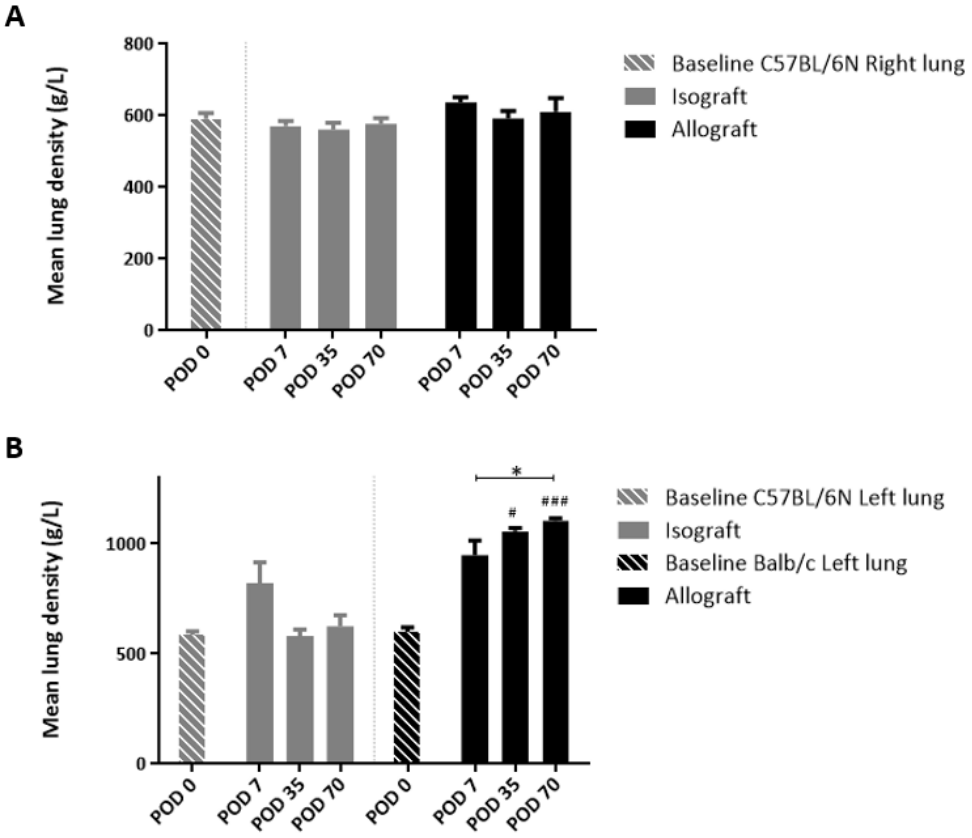

Figure 14: Mean lung density difference in allografts and isografts at POD 0, 7, 35 and 70*. (A) Graph of mean lung density of native right lungs. (B) Mean lung density of transplanted left lungs. Densities were calculated based on end-expiratory µCT images. POD: post-operative day. Error bars indicate SEM of replicate samples, n = 8 (POD 0: n = 4). * p < 0.05; # p < 0.05 compared with corresponding baseline; ### < 0.001 compared with corresponding baseline.*

4.3 Correlation between µCT and histology

µCT seems to be a useful tool to assess the disease progression given the previous results. However, the exact correlation between µCT scans and the corresponding histology, which remains the golden standard, is lacking but yet important to consider.

4.3.1 *In vivo* µCT and histology

Figure 15 illustrates the comparison between the last available *in vivo* µCT scans and the corresponding histological images. Transplanted lungs from isografts (Figure 15A) and native right lungs of allografts (Figure 15B) showed normal lung parenchyma in both µCT and histopathology. Figure 15C shows a transplanted lung of an allograft demonstrating a relatively good correlation between µCT and histology with dense, fibrotic tissue apically and at the basis a normal appearing parenchyma. The transplanted allograft of Figure 15D demonstrates high-density areas on µCT, only a small part of the main bronchus is observed while the lung parenchyma appears completely consolidated. This observation is in contrast with histology, in which the big airways are clearly visible, surrounded by parenchymal and bronchovascular fibrosis comparable to severe RAS histology. Some allografts

showed extremely high-density regions, equally to bone tissue on µCT. On histology, these regions corresponded to necrosis of lung tissue encapsulated by fibrotic tissue (Figure 15E).

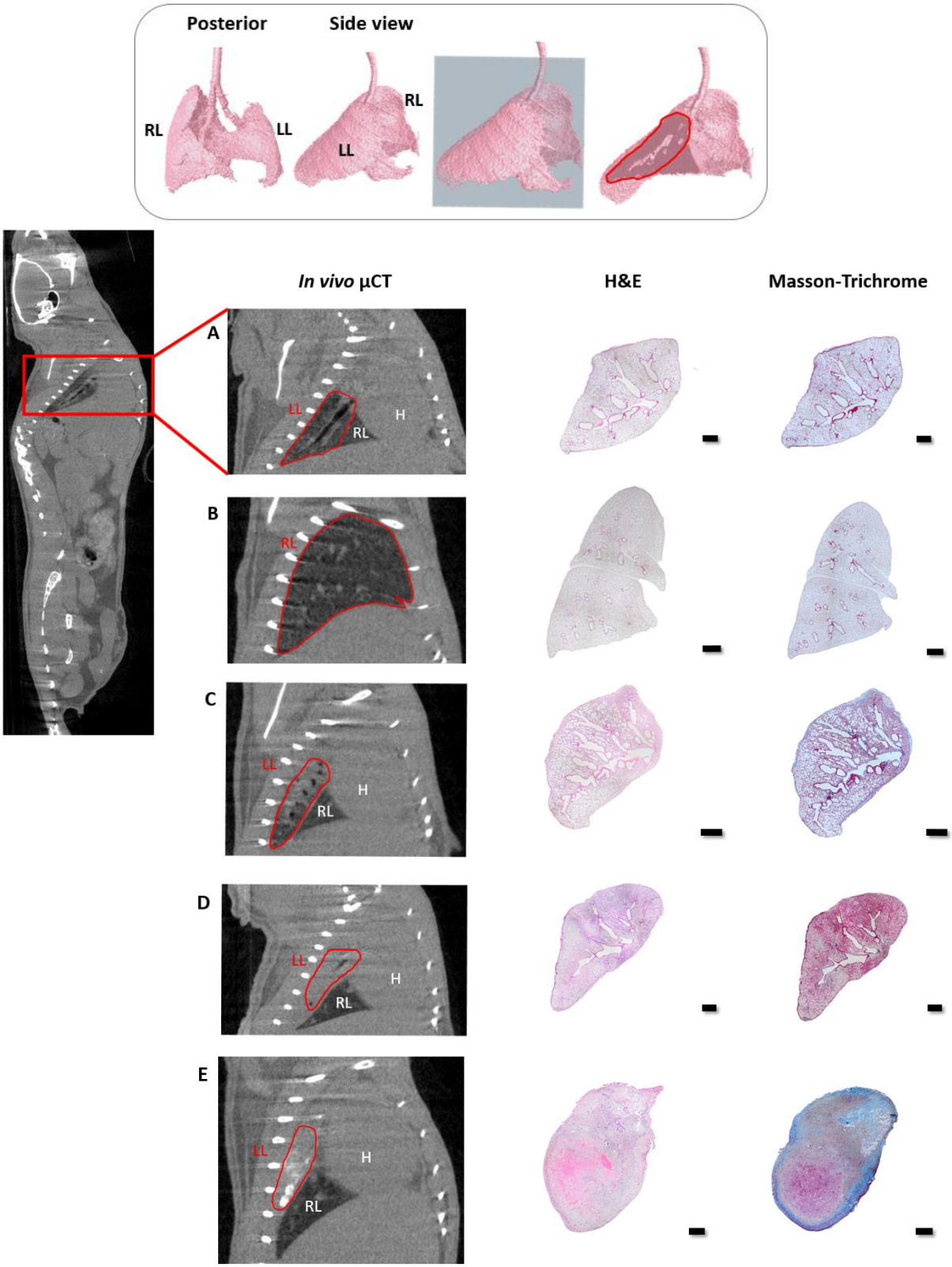

Figure 15: Comparison between in vivo µCT and histology in sagittal plane. *The tap panel shows a visualization of the sagittal plane of a 3D reconstructed left lung. (A) Transplanted lung of isograft. (B) Native, right lung of allograft. (C) (D) (E) Transplanted lungs of different allografts. Left lung is delineated in red, except in (B) where the right lung is delineated. Scale bars represent 1 mm, except of (E) 500 µm. H&E: hematoxylin and eosin; RL: right lung; H: heart LL: left lung.*

4.3.2 *Ex vivo* µCT and histology

Ex vivo µCT imaging can yield higher resolution due to the advantage of the absence of movement, a higher radiation dose and no surrounding beam distracting tissue, therefore more structural details can be observed. Figure 16 illustrates a representative *ex vivo* µCT image of an isograft (A) and allograft (B) and the corresponding histological images. *Ex vivo* µCT scans of isografts showed normal appearing lung tissue of the transplanted lung. The corresponding histology appeared normal, however cell structures appeared different due to freezing artefacts. Regarding the allografts, *ex vivo* µCT scans showed a completely consolidated transplanted lung. The histology of these scanned allografts showed complete necrosis of the transplanted lung. However, the histology was incomparable with histology of unfrozen necrotic allograft lungs.

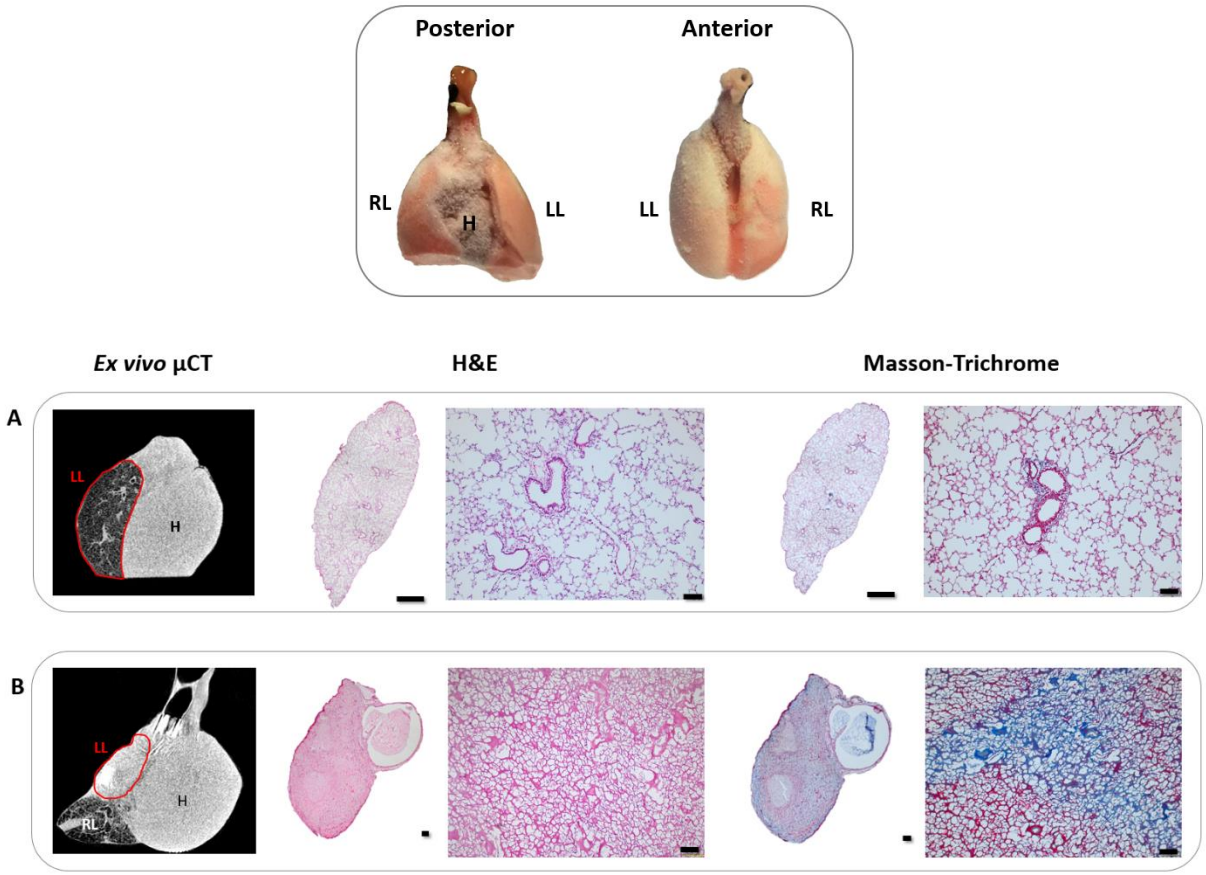

Figure 16: Ex vivo µCT versus histology in sagittal plane. *Lungs were excised and solid frozen in liquid nitrogen (upper panel). Afterwards tissues were fixated in 4% paraformaldehyde in acetone. (A) isografts; (B) allografts. The left transplanted lung is delineated in red on the ex vivo µCT scan. Scale bars of complete lungs indicate 1 mm for (A) and 200 µm for (B), of histological images indicate 100 µm. H&E: hematoxylin and eosin; RL: right lung; H: heart LL: left lung;.*

4.4 Optimizing the major mismatched orthotopic single-lung transplant model to represent human chronic rejection

Given that our previous results showed that the major antigen-mismatch orthotopic LTx mouse model with immunosuppression for ten weeks demonstrates a too severe rejection phenotype, the model was adjusted to control the rejection process with as ultimate goal to obtain a valid animal model for translational purposes. Therefore, a higher immunosuppression and a serial histological assessment was used in this second series of experiments. The higher immunosuppressive scheme consisted of the same dosage of cyclosporine and 1.6 mg/kg/day methylprednisolone (instead of 1.0 mg/kg/d). These mice were serially sacrificed at week one (n = 1), week three (n = 1), week five (n = 2) and week eight (n = 2) (Figure 17).

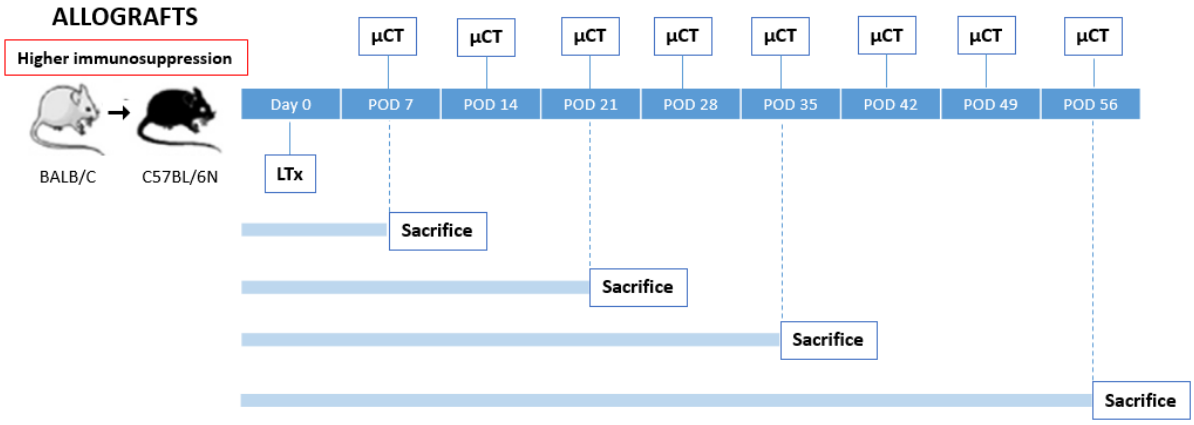

Figure 17: Study design of second experiment with higher immunosuppression. *Allografts: left LTx from Balb/c mouse to C57BL/6N mouse. POD: post-operative day; LTx: lung transplantation.*

4.2.1 Histology

Normal lung morphology was observed at POD 7, however, a lot of lymphocytic cell infiltration was already observed (Figure 18). Later, on POD 21 the transplanted lung appeared necrotic (Figure 18). At POD 35, one animal showed necrosis, the other one demonstrated preserved lung parenchyma, bronchovascular fibrosis, inflammation and (sub)pleural fibrosis (Figure 18 right). Later, at POD 56 one graft showed closed alveoli, obliterated airways and fibrosis surrounding airways and pleura (Figure 18 left). The other allograft sacrificed at POD 56 demonstrated a sharp demarcation between healthy and diseased zones of the lung with bronchovascular and pleural fibrosis, compatible with RAS (Figure 18 right).

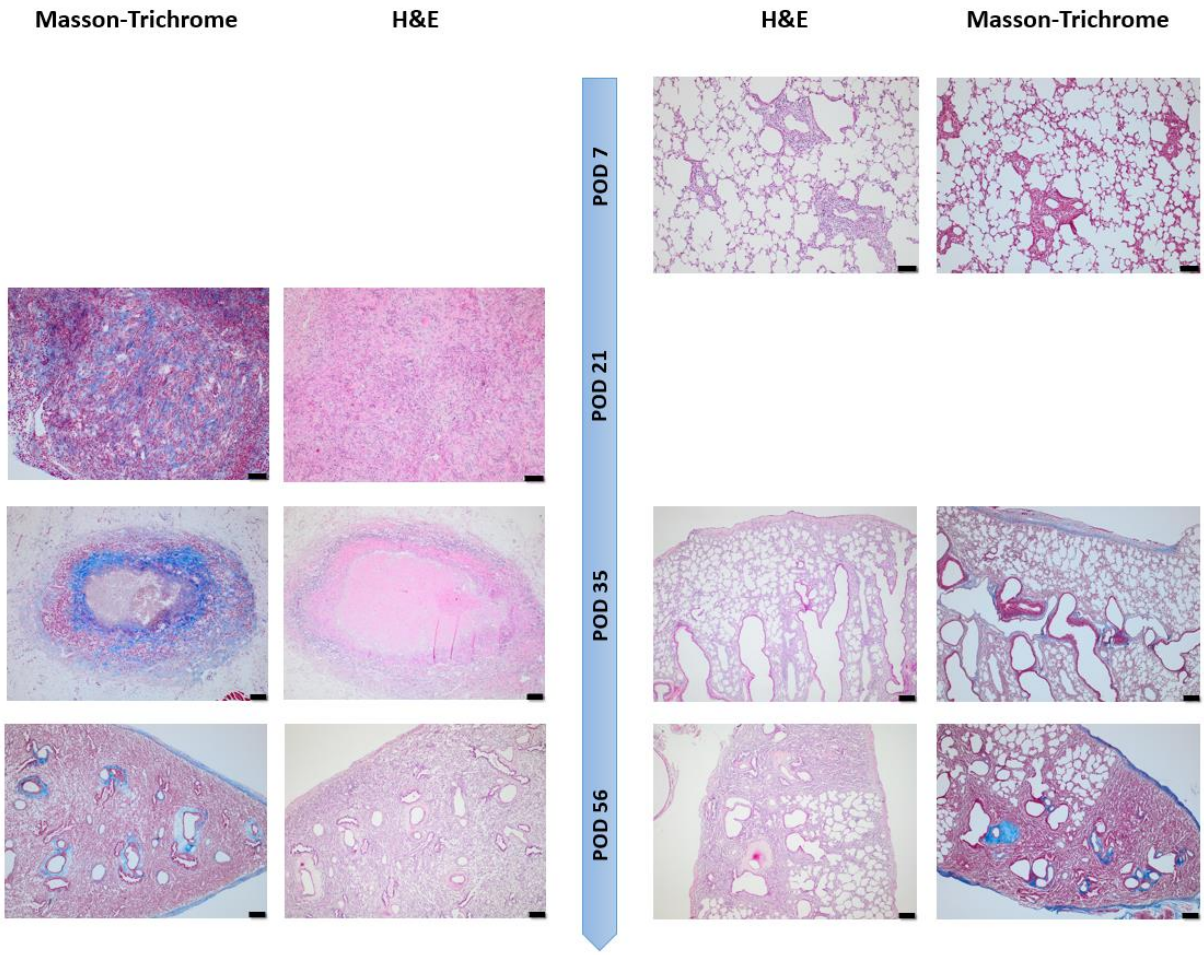

Figure 18: Evolution of histological features in LTx lung of allograft group with higher immunosuppression. *Representative images of H&E staining and Masson-Trichrome staining at POD 7, POD 21, POD 35 and POD 56. The scale bar represent 100 µm in POD 7 and POD 21 images and 200 µm in POD 35 and POD 56 images. H&E: hematoxylin and eosin; POD: post-operative day; LTx: lung transplantation.*

4.2.2 Quantification of lung volume and density

In vivo µCT scans were performed every seven days after transplantation to follow the progression of the disease. Afterwards, the scans were analyzed for lung volume and tissue density. Total lung volume of the transplanted lungs seemed to decrease over time (Figure 19A). Regarding the mean lung density, no differences were observed in the several µCT scans (Figure 19B).

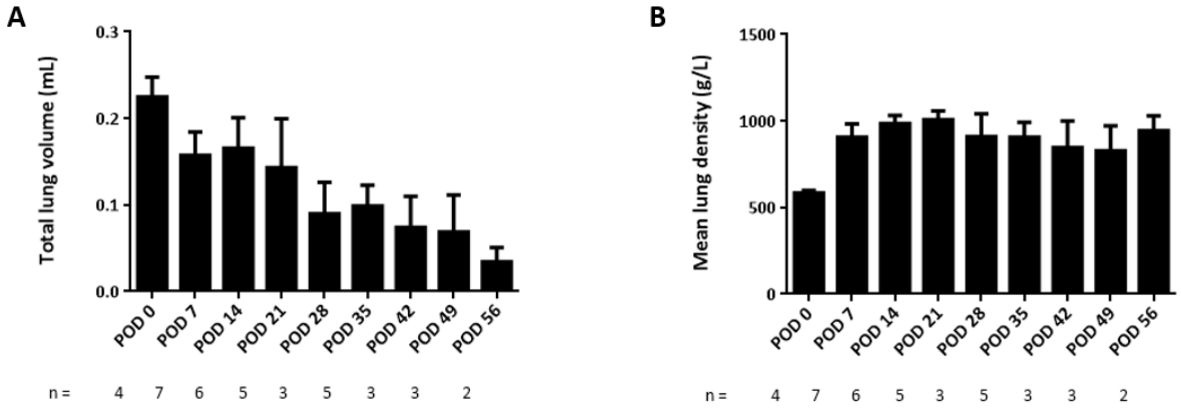

Figure 19: Total lung volume (A) and mean lung density (B) of left transplanted lungs in allografts receiving higher immunosuppression. Volumes and densities are calculated based on end-expiratory µCT images. *POD: post-operative day. Error bars indicate SEM of replicate samples.*

Compared to the initial allograft group with lower immunosuppression, it seemed that the total lung volume was higher at POD 7 and 35 in the allograft group with higher immunosuppression, however no significant differences were found (Figure 20A). The mean lung density was lower at POD 35 of the allograft group with higher immunosuppression compared to the initial allograft group with lower immunosuppression (p = 0.045) (Figure 20B).

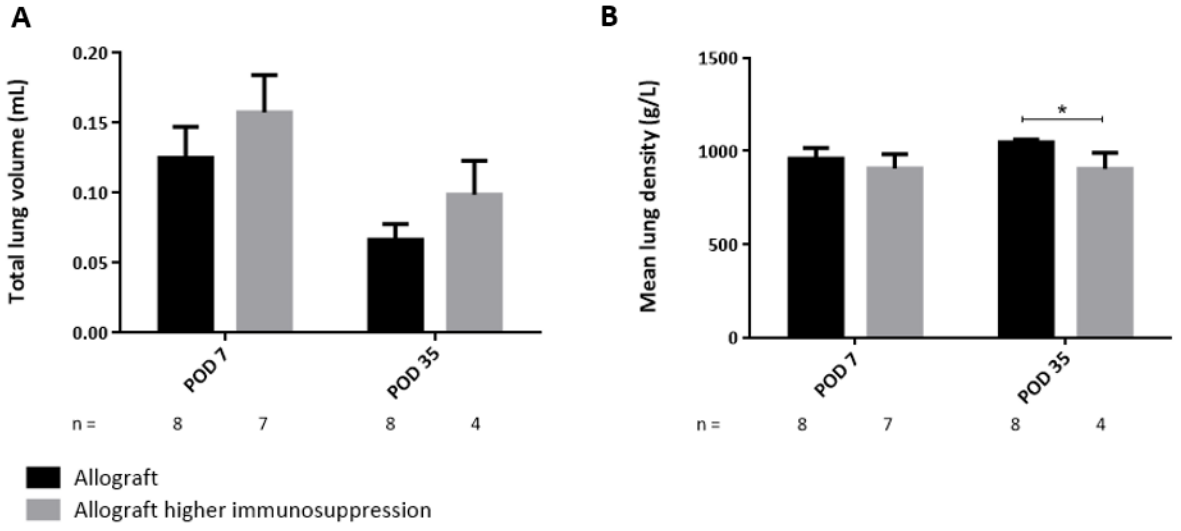

Figure 20: Comparison of total lung volume (A) and mean lung density (B) between initial allograft group and allograft group with higher immunosuppression at POD 7 and POD 35. Volumes and densities are calculated based on end-expiratory µCT images. *POD: post-operative day. Error bars indicate SEM of replicate samples.* p < 0.05.*

5. Discussion

Until now, a reproducible and relevant animal model to study chronic rejection after lung transplantation (LTx) is lacking. Since 2009, a murine orthotopic LTx model has been developed as it reflects the human procedure of a LTx more accurately. However, this animal model is used in different strain combinations for donor and recipient throughout the LTx community. Consequently, no golden standard has been accepted in the context of chronic rejection post LTx, which results in a variety of approaches to model the disease. The major antigen-mismatch combination (Balb/c → C57BL/6) is of greatest clinical relevance since major immune mismatches are also common in human LTx as genetic matching is not possible due to time and organ shortage. In addition, the transplanted mice require daily immunosuppression and is therefore the preferred animal model in this project. Hence, the aim of this study was to provide an in-depth investigation and further elaboration of the major antigen-mismatch orthotopic LTx mouse model in the context of chronic rejection and its two main phenotypes.

The murine orthotopic LTx model is currently accepted as the best model to study chronic rejection. Initially, our group established an animal model of chronic rejection with a major antigen-mismatch combination under mild immunosuppression, aiming to develop a representative model of obliterative bronchiolitis (OB). This study revealed obliterated airways in one third of the allografts ten weeks post transplantation and severe airway inflammation in the others (40). However, recently the different clinical manifestations of chronic rejection were demonstrated, including bronchiolitis obliterans syndrome (BOS) and restrictive allograft syndrome (RAS) (5). These findings led to the re-evaluation of the orthotopic LTx mouse model. Yamada *et al*. were the first to report the finding that this LTx mouse model is a model resembling RAS by means of histology (42). Later, it was demonstrated that both major and minor mismatched models showed features of RAS, with the most consistent results in the major mismatch combination (41). Therefore, the initial objective of this project was to determine how chronic rejection manifests in the major antigen-mismatch LTx mouse model. Histopathology showed a diversity of morphological changes to the allografts, ranging from severe RAS-like lesions to complete necrosis of lung tissue. These RAS-like lesions were, however observed only in one animal, represented by inflammation and fibrosis at the bronchovascular axis, near the pleura and in the parenchymal space. In addition, lymphoid follicles were observed which are exclusively detected in the RAS phenotype of chronic rejection (21). However, four other allografts showed complete necrosis of the transplanted lung, which does not represent the human disease. This might be due to complications during surgery. Another feasible explanation is that this necrosis is an advanced stage of chronic rejection. The finding that this mouse model of chronic rejection only shows features of RAS and not

BOS opens the discussion about what chronic rejection is. Our results support the idea that RAS, and not BOS, might be the primary manifestation of chronic rejection since an animal model can be studied in a controlled environment in contrast to the human situation (50). Moreover, the model will give the opportunity to further investigate the pathophysiology of RAS considering the adaptive and humoral immunity since our group already demonstrated an elevated humoral immunity in RAS compared to BOS and control lungs (21, 22). An additional advantage is that the model allows drawing blood in a longitudinal fashion. Therefore, future experiments including measuring immunoglobulins in blood of transplanted mice might help us in unraveling the disease.

Currently, the most appropriate way to assess disease progression in animal models is serial sacrifice at different time points. However, serial sacrifice is not the same as longitudinal follow-up of an individual animal. Therefore, *in vivo* imaging with micro-computed tomography (µCT) in small animal models is a powerful tool to evaluate the progression of the disease and to assess disease severity in a non-invasive way. Scans of isografts one week post-operation revealed four animals with a consolidated transplanted lung, which might be the consequence of ischemia reperfusion injury. This finding was consistent with a study by Yoshida *et al.*, showing an increased consolidation and reduced lung volume seven days after orthotopic LTx in mice by *in vivo* µCT (51). Ischemia reperfusion damage is often seen in human LTx recipients as well, denominated primary graft dysfunction (PGD). PGD is a form of acute lung injury, occurring within the first 72 hours after LTx and is caused by ischemia and preservation in donor organ and reperfusion in recipient, followed by inflammatory and immunological responses (52). However, the consolidation of the isografts at day seven post-operation could also be due to atelectasis, meaning collapse of the transplanted lung. In human recipients, this occurs when the donor lung is placed in a too small chest cavity or by bronchial stenosis (53). Preventing graft atelectasis in mouse LTx is rather difficult. However, three of these four consolidated isografts recovered on µCT scan at POD 35, indicating a capacity of the lung to recover. Therefore, arguing against lung collapse but rather partly due to a transient, reversible process comparable to PGD.

The serial µCT scans in the allograft group showed a progressive pattern of normal appearing lungs to complete consolidation, however this was only observed in a minor part of the allograft group (2/8). The remaining six allografts demonstrated complete consolidation from the first time point to the last. This might be explained by the fact that the immune mismatch leads to the body to recognize the lung as non-self, causing a massive inflammatory response, adding to the already present post-transplant damage, will lead to a completely consolidated graft. Whereas the isografts can still recover from the initial damage, the allo-immune response is too strong in the allografts. Our findings were consistent with literature: consolidation at week one for both isografts and allografts, isografts recovering after week one and allografts remaining consolidated for 28 days (48, 51, 54, 55). However, these studies

performed an additional µCT scan one day after transplantation showing normal aerated transplanted lungs, indicating a successful surgery. The lack of an earlier µCT scan after surgery is a limitation of the current study since potential surgical failures cannot be truly excluded.

Another great advantage of performing µCT scans is the possibility to quantify the images for both lung volume and mean lung density, obtaining objective and quantitative data. Total lung volume of native lungs of isografts remained stable over all three µCT scans. However, these volumes were considerably higher compared to baseline volume, indicating that immediately following transplantation the volume of the native right lung increases to compensate for the loss of function of the left transplanted lung. The total lung volumes of the transplanted lungs of the isografts confirmed this since lung volume at week one post operation was lower compared to baseline and increased in the two consecutive scans back to baseline values. This indicates that the transplanted lung from the isografts underwent ischemia reperfusion injury that will recover during later follow-up. Regarding the allografts, the increase in native lung volume is presumably due to the compensation for the loss of the left rejected lung. This also explains why pulmonary function measurements in these transplanted mice is ineffective to diagnose and assess chronic rejection since lung function will remain stable due to the expansion of the right native lung. The comparable lung function in isografts and allografts measured by repeated lung function measurements was previously described by our lab (40). As expected, the volume of the transplanted lung in the allograft group progressively declined over time. The allografts volume at POD 7 was already decreased compared to baseline volume of healthy Balb/c mice, demonstrating an extensive and rapid loss of functional lung tissue after surgery. Additionally, the right native lung increase will cause a restriction in growth to the transplanted lung and the differences in airway structures between the two strains will have an effect on the growth of the left lung (56). The decline in total lung volume of the transplanted lung was predominantly caused by a decrease in aerated lung volume. De Langhe *et al.* defined the decrease in aerated lung volume as an indicator for the extent of fibrosis in an animal model of lung fibrosis (47). µCT lung volumetry was already successfully applied in previous studies of the orthotopic LTx model to track chronic rejection (51, 57), results were consistent with the present study.

In addition to measuring lung volumes, mean lung densities were quantified as well. The transplanted left lungs from isografts showed a higher mean lung density at POD 7 compared to baseline, and restored later to normal values. These values support the volume measurements and can be explained similarly. The allografts transplanted lungs were already very dense at the first measurements and this density kept increasing over time. Although most of the allografts transplanted lungs appeared consolidated at µCT images, the mean lung density still increased indicating a further increase in the degree of fibrosis. Measuring mean lung density is important since it correlates very well with standard

readouts for fibrosis and collagen deposition. This was shown by the positive correlation between the mean lung density on µCT and the Ashcroft score and hydroxyproline content in a bleomycin-induced fibrosis mouse model, both accepted methods for estimating the extent of pulmonary fibrosis (58). In patients, physicians visually interpret CT scans, however studies exist using density as a CT-derived measurement as index of fibrotic interstitial lung disease showing that automated objective scoring is better to quantify changes in serial CT scans compared to visual scoring systems (59). Overall, quantifying lung volume and mean lung density on µCT images in small animal models allows longitudinal evaluation of dynamic changes in individual animals. A disadvantage of using *in vivo* µCT is the potential risk of radiotoxic side effects such as radiation-induced inflammation or fibrosis and carcinogenesis. The safety of using µCT in a longitudinal fashion to monitor mouse lungs was proven before, but this was for a specific shorter protocol different from ours (60). However, the isografts were scanned at the same time points as the allografts, meaning that both groups received the same radiation dose. On histology, no evidence of radiation-induced fibrosis or inflammation was observed in isografts, suggesting that the used µCT protocol is save and will not induce unwanted changes to the lungs. The overall findings related to the µCT scans in mice can be related to RAS in humans. A study by Verleden *et al.* demonstrated a significant increased density in RAS lungs compared to BOS lungs and control lungs, reflecting accumulation of scar tissue. In addition, total lung volumes of RAS lungs were lower in comparison to control lungs (26).

The third aim in this research was to investigate the correlation between µCT analysis and histopathological examination. In general, µCT scans correlated well with the corresponding histological images. Although, sometimes µCT images show a more consolidated image compared to histology. Indeed, some scans of fibrotic lungs appeared almost completely consolidated on µCT, while histology showed visible airways and parenchymal fibrosis. However, no scoring was applied for either the µCT scans or histology, therefore only descriptive and qualitative conclusions can be made without a quantitative comparison. Other studies made the same comparison but with different scoring methods for histology and µCT images. Cavanaugh *et al.* visually validated the percent lung damage in both µCT scans and corresponding histology images in a bleomycin-induced fibrosis mouse model and showed no significant differences (61). Another study compared the aerated lung volume and a consolidation assessment score, both extracted from µCT scans, to the Ashcroft-based histological score in a mouse model of pulmonary fibrosis. They showed a significant correlation between the consolidation score and the Ashcroft grading and between the aerated lung volume and the same Ashcroft scoring (62). Ideally, we would find a scoring system for µCT images of which we can deduce the corresponding histological features, but a larger number of animals are required for this.

In addition to *in vivo* µCT scans, *ex vivo* µCT scans of the extracted frozen lungs were performed since these scans can yield higher resolution compared to *in vivo* scans. The *ex vivo* µCT images of the four allografts appeared completely consolidated, yielding no extra information compared to the last *in vivo* µCT scan. The histology of the *ex vivo* scanned allografts appeared very abnormal, probably corresponding to necrosis of the graft. The freezing method induces freezing artefacts making histological interpretation difficult. Instead of freezing the lungs, it is also possible to dry the lungs with hexamethyldisilazane as demonstrated by Scotten *et al.* in a bleomycin-induced lung fibrosis animal model (63). In contrast to the freezing method, the lung will shrink and antigens will be removed during the drying process, making immunostaining impossible. Therefore, drying is inferior to the freezing method. *Ex vivo* µCT of frozen explanted lungs did not offer any advantages in the current study. However, only consolidated, necrotic lungs were scanned, perhaps if the transplanted lung would be less fibrotic, *ex vivo* µCT could be beneficial.

Taken together the results of the major antigen-mismatch orthotopic LTx mouse model with mild immunosuppression, considering the histology after ten weeks and the longitudinal follow-up using µCT, we can assume that this specific animal model demonstrates a too severe phenotype of chronic rejection. This might be due to a too low immunosuppressive scheme or a too long follow-up period. Therefore, the model was modified to resemble chronic rejection more accurately. The dosage of corticosteroid, methylprednisolone, was increased 60% since this decreases inflammation and has a general immunosuppressive function (64). Cyclosporine dosage was not changed as serum measurements of cyclosporine showed no association between the RAS-like graft and the complete necrotic lungs indicating no effect of cyclosporine. Serial sacrifice was performed which enables histological examination at different time points to assess the severity of chronic rejection. Histology at POD 7 showed rather normal lung tissue, however many lymphocytic cell infiltrates at the bronchovascular axis were already observed which indicate an episode of acute rejection. Two animals, at POD 21 and at POD 35, demonstrated complete necrosis of lung tissue. The question remains if this is due to a too fast progressing disease, complications during surgery or just the heterogeneity of the disease. Another animal sacrificed at POD 35 showed mild degree of fibrosis and inflammation, probably reflecting the onset of chronic rejection. This finding indicates that sacrifice at five weeks post operation would be too early. One allograft sacrificed at POD 56 showed end-stage disease on histology. However, the other one demonstrated regions with normal lung parenchyma, regions with inflammation, bronchovascular and (sub)pleural fibrosis presenting the desired phenotype. These results might indicate that eight weeks follow-up after LTx is more convenient instead of ten weeks. Due to time restriction, no comparison at ten weeks could be made considering histology between the initial allograft group and this allograft group with higher immunosuppression.

Furthermore, µCT scans were performed weekly to evaluate the progression of the disease and to define an appropriate endpoint. The current results showed a substantial decline in total lung volume measured over the several weeks. The mean lung density stayed stable over all µCT scans. A comparison at POD 7 and POD 35 between the two allograft groups was possible and showed a significant lower mean lung density in the transplanted lungs of the group with higher immunosuppression compared with the initial allograft group at POD 35. This finding showed a beneficial effect of the higher steroid dosage and thus seems to slow down the rejection process. Additionally, the first study about this specific animal model by our lab did not observe these necrotic lungs in a large extent, however the higher immunosuppressive scheme was used which might be an explanation (40). At the start of the present study, the immunosuppression was lowered to link it closer to the clinical situation however without the desired results. Another difference between the initial study and this one is that the C57BL/6J strain was used for the recipient mice compared to the C57BL/6N strain used in the current project. Although these only differ in substrain, substantial differences are reported in literature. C57BL/6J strain has a specific mutation that causes a defect in neutrophil recruitment whereas C57BL/6N strain has normal functioning recruitment of neutrophils (65). This difference might be important since neutrophils will be amongst the first cells to be activated following transplantation. Additionally, when extrapolating to the patient condition, neutrophils are relevant since total amount of neutrophils were increased in RAS lungs compared to control lungs and in BAL fluid of RAS patients compared to BOS patients (21, 22). In the future, a comparison should be made between the two animal strains in our model to determine which strain will give the desired outcome, more closely resembling the human disease. Considering the results of this last experiment, the higher immunosuppression might be more appropriate, although more animals are necessary to make conclusions. In addition, the exact endpoint of the follow-up has yet to be determined.

The disadvantages of this model are the high heterogeneity that affects the reproducibility, the technically difficult microsurgery and low throughput due to the long follow-up period. Perhaps, the heterogeneity can partially be explained by the surgical performance and might be diminished by improving surgical skills. Although drawbacks are related to this animal model, it remains clinically most relevant. Additionally, Yamada *et al.* confirmed that the major antigen-mismatch combination with mild immunosuppression is the most consistent in showing chronic airway fibrosis compared to other mismatch combinations (41).

Further limitations of the current study are the low n-values in the optimizing experiment of the orthotopic LTx model, making definite conclusion difficult. In addition, isografts receiving the higher immunosuppressive scheme should be considered to compare to allografts with higher immunosuppression. The histology of the *ex vivo* scanned allografts was affected due to the freezing

and fixing method, making a histological examination complicated. Furthermore, a grading of the histological images would have been helpful to show significant differences.

6. Conclusion

To conclude, the major antigen-mismatch model of orthotopic LTx represents histopathological features of RAS. However, a large amount of necrotic lungs on histopathology and complete consolidation on µCT scans of the transplanted lung was observed in the allograft group indicating a too advanced stage of chronic rejection. It seems that a higher immunosuppressive scheme might offer a solution to this problem. However, due to the current low n-values, further optimization of the model is necessary. We also demonstrated that *in vivo* µCT scanning is a useful tool to assess disease severity in a non-invasive and longitudinal fashion. An additional advantage of *in vivo* µCT is the quantification of total lung volume and mean lung density, obtaining numerical data. In contrast to *in vivo* µCT, *ex vivo* µCT did not show additional benefits in the current project. Although this was probably due to a too progressed rejected lung that was too dense to detect something on both *in vivo* and *ex vivo* µCT scans. Overall, the major antigen-mismatch combination in the orthotopic single LTx has potential to become an animal model of RAS, in which further pathological mechanisms and new therapeutic strategies can be investigated.

7. Future perspectives

The major antigen-mismatch model of murine orthotopic LTx requires further optimization to become a valid animal model for translational purposes. Once this model is completely established, it can be used for mechanistic and therapeutic studies to better understand the pathophysiological mechanisms in RAS. Emerging evidence suggests an important role for the adaptive immunity in RAS. However, regulatory cells, belonging to the adaptive immunity, might control and prevent rejection of the transplanted organ by controlling inflammation or by promoting immunological peripheral tolerance (66). Therefore, our future aim is to explore the role of regulatory cells of the adaptive immunity in this model. Our innovative approach will be an adoptive transfer of fluorescently labeled regulatory cells, allowing dynamic cell tracing with an *in vivo* imaging system (IVIS®, PerkinElmer, Zaventem, Belgium). First, the adoptive transfer will be explored and refined in the heterotopic tracheal transplant model and later fully tested in the orthotopic LTx model. Figure 21 shows pilot data of a technical potential of this approach. Regulatory T cells (T_{reg} cells) ($CD4^+$ and $CD25^+$) were isolated from a spleen via a two-step magnetic bead based cell isolation kit (Miltenyi Biotec, Leiden, The Netherlands). A first negative isolation was performed to enrich $CD4^+$ T cells from the spleen, followed by a positive selection of CD25 positive cells (the T_{reg} cells) and confirmed by flow cytometric analysis (Figure 21, green panel). Afterwards, $CD4^+$ $CD25^+$ cells (T_{reg} cells) were labeled with Yellow cell trace (ThermoFisher), confirmed by flow cytometry (Figure 21, blue panel), and intraperitoneally injected into mice (Figure 21, red panel) and visualized with an IVIS® Spectrum machine. Although the isolation protocol still needs some optimization, these provisional data demonstrates that isolating T_{reg} cells, cell labeling with tracer and tracing the cells *in vivo* is technically possible and holds promising results for the future for in depth mechanistic work regarding regulatory cells.

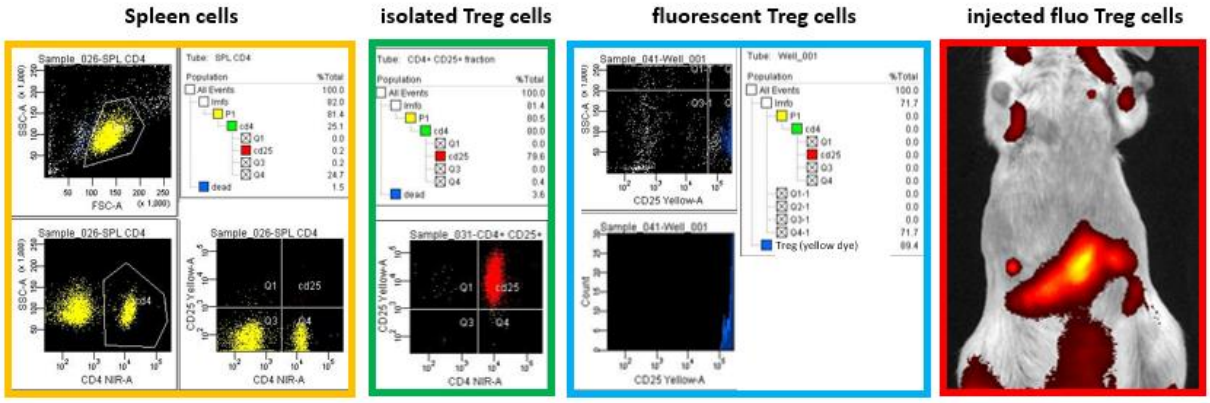

Figure 21: Pilot data of adoptive transfer of regulatory T cells. *Yellow panel demonstrates flow cytometric analysis of CD4 of the initial single cell suspension of a spleen. The green panel shows flow cytometric analysis of CD4 and CD25 of the isolated $CD4^+$ $CD25^+$ cells. The blue panel illustrates the traced $CD4^+$ $CD25^+$ cells with Yellow cell trace on flow cytometry. The last red panel shows intraperitoneal injected cells labeled with tracer into a shaved mouse. Treg cells: regulatory T cells.*

References

1. Chambers DC, Yusen RD, Cherikh WS, Goldfarb SB, Kucheryavaya AY, Khusch K, et al. The registry of the international society for heart and lung transplantation: thirty-fourth adult lung and heart–lung transplant report—2017; focus theme: allograft ischemic time. The Journal of Heart and Lung Transplantation. 2017.
2. Suwara MI, Vanaudenaerde BM, Verleden SE, Vos R, Green NJ, Ward C, et al. Mechanistic differences between phenotypes of chronic lung allograft dysfunction after lung transplantation. Transplant international : official journal of the European Society for Organ Transplantation. 2014;27(8):857-67.
3. Verleden SE, Vos R, Vanaudenaerde BM, Verleden GM. Chronic lung allograft dysfunction phenotypes and treatment. Journal of thoracic disease. 2017;9(8):2650.
4. Sato M, Keshavjee S, editors. Bronchiolitis obliterans syndrome: alloimmune-dependent and-independent injury with aberrant tissue remodeling. Seminars in thoracic and cardiovascular surgery; 2008: Elsevier.
5. Sato M, Waddell TK, Wagnetz U, Roberts HC, Hwang DM, Haroon A, et al. Restrictive allograft syndrome (RAS): a novel form of chronic lung allograft dysfunction. The Journal of Heart and Lung Transplantation. 2011;30(7):735-42.
6. Verleden GM, Raghu G, Meyer KC, Glanville AR, Corris P. A new classification system for chronic lung allograft dysfunction. Elsevier; 2014.
7. Meyer KC, Raghu G, Verleden GM, Corris PA, Aurora P, Wilson KC, et al. An international ISHLT/ATS/ERS clinical practice guideline: diagnosis and management of bronchiolitis obliterans syndrome. Eur Respiratory Soc; 2014.
8. Verleden SE, Sacreas A, Vos R, Vanaudenaerde BM, Verleden GM. Advances in understanding bronchiolitis obliterans after lung transplantation. Chest. 2016;150(1):219-25.
9. Corris PA, Ryan VA, Small T, Lordan J, Fisher AJ, Meachery G, et al. A randomised controlled trial of azithromycin therapy in bronchiolitis obliterans syndrome (BOS) post lung transplantation. Thorax. 2015;70(5):442-50.
10. Benden C, Haughton M, Leonard S, Huber LC. Therapy options for chronic lung allograft dysfunction-Bronchiolitis obliterans syndrome following first-line immunosuppressive strategies: A systematic review. The Journal of Heart and Lung Transplantation. 2017.
11. Thachuthara-George J, Crow SA, Hood CL, Bridges SA, Derksen T, Sinha N, et al. Use of alemtuzumab in the treatment of chronic lung allograft dysfunction. Transplant International. 2015;28:701.
12. Ruttens D, Verleden S, Vandermeulen E, Bellon H, Van Raemdonck D, Yserbyt J, et al. Montelukast for bronchiolitis obliterans syndrome after lung transplantation: a randomized controlled trial. The Journal of Heart and Lung Transplantation. 2016;35(4):S43-S4.
13. Verleden SE, Todd JL, Sato M, Palmer SM, Martinu T, Pavlisko EN, et al. Impact of CLAD Phenotype on Survival After Lung Retransplantation: A Multicenter Study. American journal of transplantation : official journal of the American Society of Transplantation and the American Society of Transplant Surgeons. 2015;15(8):2223-30.
14. Todd JL, Jain R, Pavlisko EN, Finlen Copeland CA, Reynolds JM, Snyder LD, et al. Impact of forced vital capacity loss on survival after the onset of chronic lung allograft dysfunction. American journal of respiratory and critical care medicine. 2014;189(2):159-66.
15. Verleden S, Vandermeulen E, Ruttens D, Vos R, Vaneylen A, Dupont L, et al., editors. Neutrophilic reversible allograft dysfunction (NRAD) and restrictive allograft syndrome (RAS). Seminars in respiratory and critical care medicine; 2013: Thieme Medical Publishers.
16. Suhling H, Dettmer S, Greer M, Fuehner T, Avsar M, Haverich A, et al. Phenotyping chronic lung allograft dysfunction using body plethysmography and computed tomography. American Journal of Transplantation. 2016;16(11):3163-70.

17. Ofek E, Sato M, Saito T, Wagnetz U, Roberts HC, Chaparro C, et al. Restrictive allograft syndrome post lung transplantation is characterized by pleuroparenchymal fibroelastosis. Modern pathology. 2013;26(3):350.
18. von der Thüsen JH, Vandermeulen E, Vos R, Weynand B, Verbeken EK, Verleden SE. The histomorphological spectrum of restrictive chronic lung allograft dysfunction and implications for prognosis. Modern Pathology. 2018.
19. Verleden SE, Ruttens D, Vandermeulen E, Bellon H, Van Raemdonck DE, Dupont LJ, et al. Restrictive chronic lung allograft dysfunction: Where are we now? : Elsevier; 2015.
20. Verleden SE, Ruttens D, Vandermeulen E, Vaneylen A, Dupont LJ, Van Raemdonck DE, et al. Bronchiolitis obliterans syndrome and restrictive allograft syndrome: do risk factors differ? Transplantation. 2013;95(9):1167-72.
21. Vandermeulen E, Lammertyn E, Verleden SE, Ruttens D, Bellon H, Ricciardi M, et al. Immunological diversity in phenotypes of chronic lung allograft dysfunction: a comprehensive immunohistochemical analysis. Transplant International. 2017;30(2):134-43.
22. Vandermeulen E, Verleden SE, Bellon H, Ruttens D, Lammertyn E, Claes S, et al. Humoral immunity in phenotypes of chronic lung allograft dysfunction: A broncho-alveolar lavage fluid analysis. Transplant immunology. 2016;38:27-32.
23. Verleden SE, Vanaudenaerde BM, Emonds MP, Van Raemdonck DE, Neyrinck AP, Verleden GM, et al. Donor-specific and -nonspecific HLA antibodies and outcome post lung transplantation. The European respiratory journal. 2017;50(5).
24. Vos R, Verleden S, Ruttens D, Vandermeulen E, Yserbyt J, Dupont L, et al. Pirfenidone: a potential new therapy for restrictive allograft syndrome? American Journal of Transplantation. 2013;13(11):3035-40.
25. Suhling H, Bollmann B, Gottlieb J. Nintedanib in restrictive chronic lung allograft dysfunction after lung transplantation. The Journal of Heart and Lung Transplantation. 2016;35(7):939-40.
26. Verleden SE, Vasilescu DM, McDonough JE, Ruttens D, Vos R, Vandermeulen E, et al. Linking clinical phenotypes of chronic lung allograft dysfunction to changes in lung structure. European Respiratory Journal. 2015:ERJ-00106-2015.
27. Hele DJ, Yacoub MH, Belvisi MG. The heterotopic tracheal allograft as an animal model of obliterative bronchiolitis. Respiratory research. 2001;2(3):169.
28. Dutly AE, Andrade CF, Verkaik R, Kugathasan L, Trogadis J, Liu M, et al. A Novel Model for Post-Transplant Obliterative Airway Disease Reveals Angiogenesis from the Pulmonary Circulation. American journal of transplantation. 2005;5(2):248-54.
29. Sung SH, Warnock M, Fang KC, Hall KW, Hall TS. A comparison of rat tracheal transplant models: implantation verses anastomotic techniques for the study of airway rejection1. Transplantation. 2002;73(5):695-700.
30. Sato M, Keshavjee S, Liu M. Translational research: animal models of obliterative bronchiolitis after lung transplantation. American Journal of Transplantation. 2009;9(9):1981-7.
31. Veith FJ, Richards K. Improved technic for canine lung transplantation. Annals of surgery. 1970;171(4):553.
32. Hämmäinen PT. Single Lung Transplantation in Piglets: Technique and Follow-up. Scandinavian journal of thoracic and cardiovascular surgery. 1993;27(2):71-80.
33. Castaneda A, Arnar O, Schmidt-Habelman P, Moller J, Zamora R. Cardiopulmonary autotransplantation in primates. The Journal of cardiovascular surgery. 1972;13(5):523.
34. Sui H, Olivier A, Klesney-Tait J, Brooks L, Tyler S, Sun X, et al. Ferret lung transplant: an orthotopic model of obliterative bronchiolitis. American Journal of Transplantation. 2013;13(2):467-73.
35. Jungraithmayr W, Vogt P, Inci I, Hillinger S, Arni S, Korom S, et al. A model of chronic lung allograft rejection in the rat. European Respiratory Journal. 2010;35(6):1354-63.
36. Okazaki M, Krupnick A, Kornfeld C, Lai J, Ritter J, Richardson S, et al. A mouse model of orthotopic vascularized aerated lung transplantation. American Journal of Transplantation. 2007;7(6):1672-9.

37. Okazaki M, Gelman AE, Tietjens JR, Ibricevic A, Kornfeld CG, Huang HJ, et al. Maintenance of airway epithelium in acutely rejected orthotopic vascularized mouse lung transplants. American journal of respiratory cell and molecular biology. 2007;37(6):625-30.
38. Fan L, Benson HL, Vittal R, Mickler EA, Presson R, Fisher AJ, et al. Neutralizing IL-17 Prevents Obliterative Bronchiolitis in Murine Orthotopic Lung Transplantation. American Journal of Transplantation. 2011;11(5):911-22.
39. Hogan BL, Barkauskas CE, Chapman HA, Epstein JA, Jain R, Hsia CC, et al. Repair and regeneration of the respiratory system: complexity, plasticity, and mechanisms of lung stem cell function. Cell stem cell. 2014;15(2):123-38.
40. De Vleeschauwer S, Jungraithmayr W, Wauters S, Willems S, Rinaldi M, Vaneylen A, et al. Chronic rejection pathology after orthotopic lung transplantation in mice: the development of a murine BOS model and its drawbacks. PLoS One. 2012;7(1):e29802.
41. Yamada Y, Windirsch K, Dubs L, Kenkel D, Jang J-H, Inci I, et al. Chronic Airway Fibrosis in Orthotopic Mouse Lung Transplantation Models-An Experimental Reappraisal. Transplantation. 2017.
42. Yamada Y, Vandermeulen E, Heigl T, Somers J, Vaneylen A, Verleden S, et al. The role of recipient derived interleukin-17A in a murine orthotopic lung transplant model of restrictive chronic lung allograft dysfunction. Transplant immunology. 2016;39:10-7.
43. Lama VN, Belperio JA, Christie JD, El-Chemaly S, Fishbein MC, Gelman AE, et al. Models of Lung Transplant Research: a consensus statement from the National Heart, Lung, and Blood Institute workshop. JCI insight. 2017;2(9).
44. Jungraithmayr W, Jang J-H, Schrepfer S, Inci I, Weder W. Small animal models of experimental obliterative bronchiolitis. American journal of respiratory cell and molecular biology. 2013;48(6):675-84.
45. Velde GV, Poelmans J, De Langhe E, Hillen A, Vanoirbeek J, Himmelreich U, et al. Longitudinal micro-CT provides biomarkers of lung disease and therapy in preclinical models, thereby revealing compensatory changes in lung volume. Disease Models & Mechanisms. 2015:dmm. 020321.
46. Li M, Jirapatnakul A, Biancardi A, Riccio ML, Weiss RS, Reeves AP. Growth pattern analysis of murine lung neoplasms by advanced semi-automated quantification of micro-CT images. PLoS One. 2013;8(12):e83806.
47. De Langhe E, Velde GV, Hostens J, Himmelreich U, Nemery B, Luyten FP, et al. Quantification of lung fibrosis and emphysema in mice using automated micro-computed tomography. PLoS One. 2012;7(8):e43123.
48. Wurnig MC, Tsushima Y, Weiger M, Jungraithmayr W, Boss A. Assessing lung transplantation ischemia-reperfusion injury by microcomputed tomography and ultrashort echo-time magnetic resonance imaging in a mouse model. Investigative radiology. 2014;49(1):23-8.
49. National Research Council Committee for the Update of the Guide for the C, Use of Laboratory A. The National Academies Collection: Reports funded by National Institutes of Health. In: th, editor. Guide for the Care and Use of Laboratory Animals. Washington (DC): National Academies Press (US)

National Academy of Sciences.; 2011.
50. Vanaudenaerde B, Verleden S, Neyrinck A, Verleden G, Vos R. A New Step in the Marathon of Understanding Chronic Rejection after Lung Transplantation. Am Thoracic Soc; 2017.
51. Yoshida M, Oishi H, Martinu T, Hwang DM, Takizawa H, Sugihara J, et al. Pentraxin 3 deficiency enhances features of chronic rejection in a mouse orthotopic lung transplantation model. Oncotarget. 2018;9(9):8489.
52. Morrison MI, Pither TL, Fisher AJ. Pathophysiology and classification of primary graft dysfunction after lung transplantation. Journal of thoracic disease. 2017;9(10):4084.
53. Chia E, Babawale SN. Imaging features of intrathoracic complications of lung transplantation: What the radiologists need to know. World Journal of Radiology. 2017;9(12):438.
54. Hirayama S, Sato M, Loisel-Meyer S, Matsuda Y, Oishi H, Guan Z, et al. Lentivirus IL-10 Gene Therapy Down-Regulates IL-17 and Attenuates Mouse Orthotopic Lung Allograft Rejection. American Journal of Transplantation. 2013;13(6):1586-93.

55. Zhou W, Zhou X, Gaowa S, Meng Q, Zhan Z, Liu J, et al. The critical role of induced CD4+ FoxP3+ regulatory cells in suppression of interleukin-17 production and attenuation of mouse orthotopic lung allograft rejection. Transplantation. 2015;99(7):1356-64.
56. Thiesse J, Namati E, Sieren JC, Smith AR, Reinhardt JM, Hoffman EA, et al. Lung structure phenotype variation in inbred mouse strains revealed through in vivo micro-CT imaging. Journal of Applied Physiology. 2010;109(6):1960-8.
57. Oishi H, Martinu T, Sato M, Matsuda Y, Hirayama S, Juvet SC, et al. Halofuginone treatment reduces interleukin-17A and ameliorates features of chronic lung allograft dysfunction in a mouse orthotopic lung transplant model. The Journal of Heart and Lung Transplantation. 2016;35(4):518-27.
58. Velde GV, De Langhe E, Poelmans J, Dresselaers T, Lories RJ, Himmelreich U. Magnetic Resonance Imaging for Noninvasive Assessment of Lung Fibrosis Onset and Progression: Cross-Validation and Comparison of Different Magnetic Resonance Imaging Protocols With Micro–Computed Tomography and Histology in the Bleomycin-Induced Mouse Model. Investigative radiology. 2014;49(11):691-8.
59. Hansell DM, Goldin JG, King Jr TE, Lynch DA, Richeldi L, Wells AU. CT staging and monitoring of fibrotic interstitial lung diseases in clinical practice and treatment trials: a position paper from the Fleischner Society. The Lancet Respiratory Medicine. 2015;3(6):483-96.
60. Vande Velde G, De Langhe E, Poelmans J, Bruyndonckx P, d'Agostino E, Verbeken E, et al. Longitudinal in vivo microcomputed tomography of mouse lungs: no evidence for radiotoxicity. American Journal of Physiology-Lung Cellular and Molecular Physiology. 2015;309(3):L271-L9.
61. Cavanaugh D, Travis EL, Price RE, Gladish G, White RA, Wang M, et al. Quantification of bleomycin-induced murine lung damage in vivo with micro-computed tomography. Academic radiology. 2006;13(12):1505-12.
62. Rodt T, von Falck C, Dettmer S, Halter R, Maus R, Ask K, et al. Micro-computed tomography of pulmonary fibrosis in mice induced by adenoviral gene transfer of biologically active transforming growth factor-β1. Respiratory research. 2010;11(1):181.
63. Scotton CJ, Hayes B, Alexander R, Datta A, Forty EJ, Mercer PF, et al. Ex vivo micro-computed tomography analysis of bleomycin-induced lung fibrosis for preclinical drug evaluation. The European respiratory journal. 2013;42(6):1633-45.
64. Barnes PJ. How corticosteroids control inflammation: quintiles prize lecture 2005. British journal of pharmacology. 2006;148(3):245-54.
65. Ulland TK, Jain N, Hornick EE, Elliott EI, Clay GM, Sadler JJ, et al. Nlrp12 mutation causes C57BL/6J strain-specific defect in neutrophil recruitment. Nature communications. 2016;7:13180.
66. Wood KJ, Bushell A, Hester J. Regulatory immune cells in transplantation. Nature Reviews Immunology. 2012;12(6):417.

Supplemental data

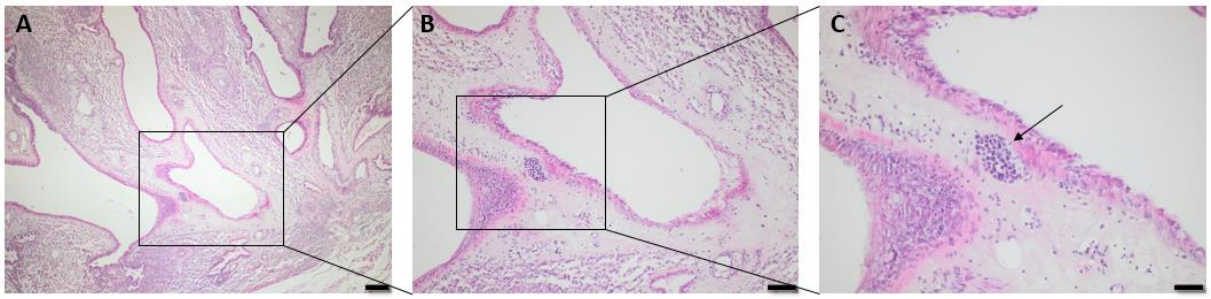

Figure 22S: Hematoxylin and eosin staining of lymphoid follicle in RAS-like allograft lung ten weeks post-transplantation. *Arrow indicate lymphoid follicle. Scale bar of (A) indicate 200 µm, of (B) 100 µm and of (C) 50 µm. RAS: restrictive allograft syndrome.*

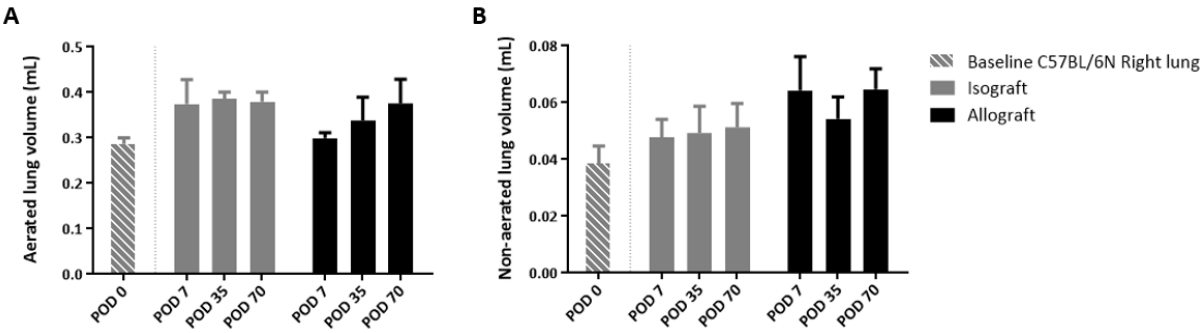

Figure 23S: Aerated (A) and non-aerated lung volumes (B) of native right lung in isografts and allografts at POD 0, 7, 35 and 70. *Volumes are calculated based on end-expiratory µCT images. POD: post-operative day.*

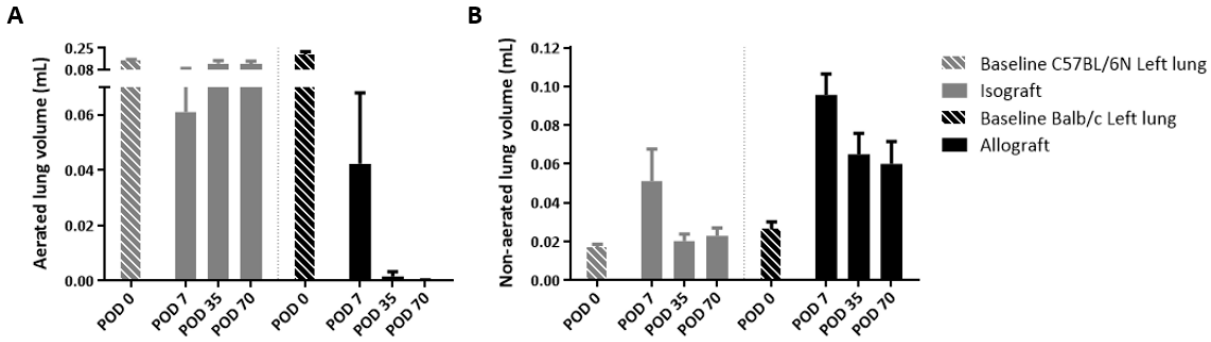

Figure 24S: Aerated (A) and non-aerated lung volumes (B) of transplanted left lung in isografts and allografts at POD 0, 7, 35 and 70. *Volumes are calculated based on end-expiratory µCT images. POD: post-operative day.*

Auteursrechtelijke overeenkomst

Ik/wij verlenen het wereldwijde auteursrecht voor de ingediende eindverhandeling:
A closer look at chronic rejection in the murine model of orthotopic lung transplantation

Richting: **Master of Biomedical Sciences-Clinical Molecular Sciences**
Jaar: **2018**

in alle mogelijke mediaformaten, - bestaande en in de toekomst te ontwikkelen - , aan de Universiteit Hasselt.

Niet tegenstaand deze toekenning van het auteursrecht aan de Universiteit Hasselt behoud ik als auteur het recht om de eindverhandeling, - in zijn geheel of gedeeltelijk -, vrij te reproduceren, (her)publiceren of distribueren zonder de toelating te moeten verkrijgen van de Universiteit Hasselt.

Ik bevestig dat de eindverhandeling mijn origineel werk is, en dat ik het recht heb om de rechten te verlenen die in deze overeenkomst worden beschreven. Ik verklaar tevens dat de eindverhandeling, naar mijn weten, het auteursrecht van anderen niet overtreedt.

Ik verklaar tevens dat ik voor het materiaal in de eindverhandeling dat beschermd wordt door het auteursrecht, de nodige toelatingen heb verkregen zodat ik deze ook aan de Universiteit Hasselt kan overdragen en dat dit duidelijk in de tekst en inhoud van de eindverhandeling werd genotificeerd.

Universiteit Hasselt zal mij als auteur(s) van de eindverhandeling identificeren en zal geen wijzigingen aanbrengen aan de eindverhandeling, uitgezonderd deze toegelaten door deze overeenkomst.

Voor akkoord,

Kaes, Janne

Datum: **7/06/2018**